International Journal of Multiphase Flow 189 (2025) 105239

Contents lists available at ScienceDirect

International Journal of Multiphase Flow

journal homepage: www.elsevier.com/locate/ijmulflow

50 Years of International Journal of Multiphase Flow: Experimental methods for dispersed multiphase flows

Laura Villafañe [a], Alberto Aliseda [b], Steven Ceccio [c], Paolo Di Marco [d], Nathanaël Machicoane [e], Theodore J. Heindel [f,*]

[a] Department of Aerospace Engineering, University of Illinois Urbana-Champaign, Urbana, IL, 61801, USA
[b] Department of Mechanical Engineering, University of Washington, Seattle, WA, 98195-2600, USA
[c] Mechanical Engineering & Applied Mechanics, University of Michigan, Ann Arbor, MI, 48109-2102, USA
[d] Department of Energy, Systems, Constructions and Territory Engineering, University of Pisa, 56122, Pisa, Italy
[e] Univ. Grenoble Alpes, CNRS, Grenoble INP, LEGI, 38000, Grenoble, France
[f] Center for Multiphase Flow Research and Education and Department of Mechanical Engineering, Iowa State University, Ames, IA, 50011-2274, USA

ARTICLE INFO

Keywords:
Experimental methods
Experimental techniques
New research development and opportunities
Review

ABSTRACT

The presence of one or more dispersed phases in a continuous carrier flow adds challenges to the experimental characterization of multiphase flows. Numerous experimental techniques have been developed over the past 50 years that overcome the challenges introduced by the optical opacity and the presence of phase interfaces, some providing global quantities while others offering local or spatial information of the distinct phases. This paper reviews several experimental techniques for dispersed multiphase flow measurements that are relevant to various types of flows with a gaseous, solid, or liquid phase dispersed in a gas or liquid carrier, and that are considered important by the authors based on their collective experience. Additionally, the paper highlights promising areas of ongoing development aimed at advancing multiphase flow measurement techniques.

1. Introduction

Dispersed multiphase flows are ubiquitous, from natural and industrial processes to consumer products and daily activities. Rain, ash in volcanic eruptions, sandstorms, sediments and microplastics in environmental flows, are a few examples of a dispersed phase transported in a continuous carrier phase. Industrial applications relying on multiphase flows include chemical and fuel production, energy conversion, and beverage and food processing. Characterizing these multiphase environments typically involves quantifying the properties and behavior of the discrete phase (or phases) and those of the carrier flow. Measurements may include dispersed phase particle or bubble size and shape, local volume fraction, and dispersed and continuous phase velocities. Other measures of interest for system performance are global in nature such as regime identification, overall pressure drop, average diffusion coefficients, heat and mass transfer rates, dispersed phase residence time, and power consumption. In all cases, measurements are needed to monitor and optimize process conditions as well as to develop empirical correlations, inspire first-principal models, and validate computational tools.

Multiphase flow measurement techniques have been reviewed in multiple publications. Since the seminal work by Hewitt describing a wide range of methods for two-phase flows (Hewitt, 1978), several review works have documented the progress on experimental techniques over the past decades (Bachalo, 1994; Powell, 2008; Snoek, 1990) with most recent reviews focusing on field imaging techniques (Hampel, 2023; Poelma, 2020). A comprehensive background on dispersed multiphase flows, including experimental and modeling approaches, and perspectives, is available (Balachandar, 2024; Balachandar and Eaton, 2010; Brandt and Coletti, 2022; Capecelatro and Wagner, 2024; Ni, 2024; Subramaniam, 2020). The current work provides a summary of the types of experimental techniques developed over the last 50 years that are of interest and important to the authors with the aim to give a perspective on what experimental developments are being advanced, and where new progress is needed to improve the science and technology of dispersed multiphase flows. Our focus is on the measurement of various characteristics of gas, solid, or liquid inclusions in a gas or liquid carrier phase, at volume loadings spanning from very dilute to dense

* Corresponding author.
E-mail addresses: lvillafa@illinois.edu (L. Villafañe), aaliseda@u.washington.edu (A. Aliseda), ceccio@umich.edu (S. Ceccio), paolo.dimarco@unipi.it (P. Di Marco), nathanael.machicoane@univ-grenoble-alpes.fr (N. Machicoane), theindel@iastate.edu (T.J. Heindel).

https://doi.org/10.1016/j.ijmultiphaseflow.2025.105239
Received 13 October 2024; Received in revised form 23 March 2025; Accepted 30 March 2025
Available online 5 April 2025
0301-9322/

regimes. Techniques included in this work span invasive probes and optical and laser-based imaging, which are more suitable to dilute flows, to soft- and hard-field electromagnetic sensing methods, which can provide measurements in particle-dense flow regimes. The reference list used in the review is extensive, but not all-inclusive. Following the description of the techniques of interest, a discussion on emerging new developments and future areas of opportunity is presented, prior to brief concluding remarks.

2. Current state-of-the-art experimental techniques

2.1. Invasive probes

Invasive probes typically apply to gas or liquid dispersed phases and are designed such that the signal produced by the dispersed and carrier phases differs significantly, and such that the sensing element is small enough to minimally affect the local environment. Interpretation of the signal must consider the local interaction of the probe with the interface between phases, and this is strongly dependent on the probe size compared to the relevant length scale of the dispersed phase (e.g., the bubble size (Guet et al., 2003; Yamada and Saito, 2012)). Interfaces may be deformed by the probe, and the path of small inclusions may deviate as they encounter the probe (Cartellier and Achard, 1991; Vejražka et al., 2010). Careful calibration of these probes using high-speed imaging is often necessary to correctly interpret the probe signal. Selected examples of the different invasive probes are described below.

2.1.1. Hot wire

Hot wire (and hot film) anemometry systems for the measurement of dispersed phase volume fractions, dispersed phase passing time, and dispersed phase and carrier phase velocity statistics have traditionally been carried out with a common Wheatstone bridge in constant temperature mode. This takes advantage of the extreme differences in convective heat transfer coefficients associated with the differences in density between phases. Furthermore, the stability of the Wheatstone bridge signal allows for accurate differentiation between the signals associated with the two phases, and the preservation of the signal, without overshoots, to reconstruct the maximum amount of carrier flow velocity signal during passage of dispersed phase inclusions (Abel and Resch, 1978; Farrar and Bruun, 1989). Hence, due to the different thermal capacity of the different phases, the hot wire anemometer signal undergoes a very fast transition in liquid/gas systems, and to a certain degree also in liquid/liquid systems, making the detection of the time of arrival of the phase interface at the tip of the probe an accurate and reliable measurement. As the dispersed phase leaves the probe, an inverse transition in the signal occurs, pinpointing the time when the second interface passes. Based on this basic principle, three different types of measurements are possible, and have been made: local void fraction (Abel and Resch, 1978; Delhaye, 1969; Toral, 1981), bubble or droplet size or chord length (Bremhorst and Gilmore, 1976; Farrar and Bruun, 1989), and local velocity of the continuous or dispersed phase (Bruun, 1995; Farrar et al., 1995; Zenit et al., 2001).

2.1.2. Optical

An optical probe generally uses a fiber optics-based endoscope to illuminate the flow and collect the light scattered by the dispersed phase. The scattered light is then used to extract the Doppler shift frequency or amplitude signal, that can be related to the residence time, size, or velocity of the dispersed phase. Coherent light has inherent advantages to extracting information, but many different light preconditioning setups can be used to enhance the measurements, such as multiplexing in time or in frequency. Optical probes have been used to quantify the volume fraction of a dispersed gas phase in a continuous carrier fluid through chord length measurements. The principle is simple and parallels that of the hot wire measurements: track the signal as a function of time and differentiate the response in the dispersed phase from the continuous phase. The percentage of time in the dispersed flow can be converted to a volume fraction, with thresholding of the signal based on its intensity to account for the time when the bubble/droplet is transecting the probe (not the approach period), and assuming that continuous and dispersed phases have the same mean velocity. More refined versions of the signal processing replace intensity thresholding with light phase shifts to identify transitions between phases on the optical signal profiting from the 180 degrees phase change in the reflected light when the optical probe is emitting while immersed in the continuous phase or in the dispersed phase (Alonzo et al., 2023; Cartellier, 1992b; Cartellier and Achard, 1991; Lefebvre et al., 2022). The transit time can then be clearly identified, without the need of sensitive intensity thresholds accounting for bubble proximity. Assumptions about the bubbles transecting the optical signal along their diameter, and of the bubble velocity, allow bubble diameters and dispersed phase volume fraction to be estimated. Alternatively, the optical signal can be used to measure the bubble velocity by using amplitude or frequency modulation of the recorded signal when coherent light is used, or via the Doppler shift of the scattered light (Alonzo et al., 2023; Cartellier, 1992a; Lefebvre et al., 2022).

2.1.3. Electrical impedance probes

Measurement of a substance's electrical impedance may also be used to discern the interface between different phases of a multiphase flow. In a typical application, one or more sharp electrodes ("needles") are inserted into the flow. Each needle is sheathed in a grounded outer housing separated from the needle by an electrically insulated layer. A circuit is made between the tip of the needle and the grounded housing (or another nearby needle), with current passing through the fluid (Munholand and Soucy, 2005). These probes are referred to as resistance, capacitance, or impedance probes, depending on what provides the highest contrast based on the properties of the continuous and dispersed phases. Resistance probes are employed when the contrast in phases is dominated by the difference in resistivity (e.g., tap water and air). Capacitive probes are used when the contrast is mainly due to changes in the reactivity and in the absence of significant inductive effects (e.g., hydrocarbons and air). Resistance probes may have carrier frequencies on the order of 1 to 100s of kHz, while capacitive probes typically have carrier frequencies on the order of 100 kHz or higher (Ceccio and George, 1996). An impedance probe can be used to measure both the resistive and reactive components of the material impedance (Monrós-Andreu et al., 2016). Similar to hot wire and optical probes, it is possible to detect the passage of phase boundaries through the probe if the distinct phases have significantly different electrical impedances.

Signal processing of the probe output is a critical element of these setups. The time variation of the signal from a single-point probe can be used to estimate the local volume fraction (Leung et al., 1995). Multi-point probes can use time-of-flight information to estimate interfacial velocity and area concentration and other higher-order position and velocity correlations (Da Silva et al., 2007; Monrós-Andreu et al., 2016; Zhao et al., 2005).

Electrical impedance probes may also be used to determine the bulk average properties of a multiphase mixture (Ceccio and George, 1996). In this case, the probe is used to measure the average impedance of the mixture in each interrogation volume from which the local volume fraction is then inferred. Direct calibration can be used (e.g., measurement of each individual phase, such as liquid and gas), or the fraction of a dispersed mixture can be computed based on the impedance for each material phase along with a mixture model, such as the Maxwell-Hewitt relationship (George et al., 2000b; Peña and Rodriguez, 2015; Torczynski et al., 1995). Both needle point and surface mounted electrode configurations can be used for bulk impedance measurements (Cho et al., 2005; Elbing et al., 2008; George et al., 2000a). Da Silva (Da Silva, 2008) presents a review of impedance-based probes.

It is possible to combine several simultaneous point-wise measurements to map the 2D or 3D distribution of the impedance and, when interpolated, the field properties of the multiphase flow. This can be accomplished with an array of individual probes or compound probes with multiple sensing elements. It is also possible to create a matrix of local impedance measurements using an array of crossed wires to create a "wire mesh sensor" (Li et al., 2025; Prasser et al., 2001). Reviews of these techniques are available (Peña and Rodriguez, 2015; Tompkins et al., 2018). Significant consideration must be given to the effect that the wire mesh sensors may have on the flow itself at both the scale of the mesh points and across the entire measurement plane.

2.2. Imaging methods

2.2.1. Backlit and shadowgraphy

While the designations of backlit and shadowgraphy are often used interchangeably, shadowgraphy is a type of backlit imaging where collimated light is used for volumetric illumination instead of the diverging light source typically used in backlit imaging. In both cases, the measurement volume is located between the illumination source and the lens system of the camera collecting the images. Visible light is largely reflected and refracted by an object, hence creating a shadow. As such, these techniques inform of the presence or absence of an obstacle along the light beam path, but not generally on the obstacle depth along the beam path. Depending on the illumination and on the dispersed objects, a dark shadow may form on the imaging sensor, or light can be refracted in such a way that the center of the object appears bright, even brighter than the background if light focusing occurs (Bothell et al., 2020). Optical backlit imaging methods work well for bubbles, which often challenge side illumination (light scattering), with image processing used to fill bright internal regions in their image projections (Pillers and Heindel, 2023). The resulting shadowgraphy or backlit images show low-intensity pixels revealing the shape of objects projected on the plane perpendicular to the beam path, as shown in Fig. 1. Changes in the illumination configuration, such as the use of spatial filtering or coherent light, can convert a shadowgraphy setup into that required for Schlieren or holography, respectively (Tropea et al., 2007).

In backlit imaging, a diverging light source is typically used. When precisely determining an interface location in a complex 3D multiphase flow, a small depth of field is preferred (Fig. 1b) (Ricard et al., 2021), making it possible to measure the projected spatial extent of a liquid jet (Tolfts et al., 2023) in one or two orthogonal projections by duplicating the setup (Kaczmarek et al., 2022). Small depth of field and high magnification can capture sharp edges between two interfaces, critical to computing phase presence probability maps (Machicoane et al., 2020) and droplet size measurements. Large depth of field may be preferred in other imaging applications like particle tracking velocimetry with single or multi-camera setups (Machicoane et al., 2014; Tan et al., 2020; Toschi and Bodenschatz, 2009).

A collimated light source is used for shadowgraphy, which is commonly afocal, i.e. yielding an infinite depth of field. While this is impractical when imaging an optically dense flow like the near-field region of a spray, shadowgraphy is ideal for object sizing in dilute multiphase flows (Fdida and Blaisot, 2009) and when the measurement volume is large (Machicoane et al., 2013), since the size of the object on the image plane does not depend on its position within the measurement volume (Fig. 1a). This lack of size sensitivity to in-depth position facilitates camera calibrations and can be used to perform 3D particle tracking with only two orthogonal cameras and without the need of powerful illumination sources (Huck et al., 2017).

2.2.2. Liquid-vapor phase detection at the wall

Optical measurements provide useful quantitative information in near-wall gas-liquid flows. The liquid can form a thin film in contact with the surface or can appear at the base of a growing bubble (microlayer). The determination of the film thickness is of paramount importance for measurement and modeling of local wall heat flux and shear stress found in phase change. Several optical techniques have been proposed to characterize wall contact (Kossolapov et al., 2021). Other techniques like micro-thermometers, time-domain thermos-reflectance, and confocal sensors provide excellent time resolution but are limited to pointwise measurements.

Techniques using visible light are the most promising and economical for measuring wall vapor/liquid film thickness. Differences of refraction index between the vapor and liquid phases allow detecting microlayers by thin-film fringe interferences when illumination is provided by a coherent laser source. The challenges with this approach are the possible appearance of parasitic interference patterns or laser speckle patterns, and its sensitivity to parallelism of the substrate faces (Koffman and Plesset, 1983). To mitigate these effects, incoherent broadband light has been used to exploit total internal reflection (Nishio et al., 1998; Surtaev et al., 2018). White light interferometry has also been used to measure the microlayer thickness (Glovnea et al., 2003; Tecchio et al., 2024). Finally, a monochromatic, narrow-band visible light source can also be used, which has only recently become possible with the development of powerful LED lights (Kossolapov et al., 2021). As shown in Fig. 2, the presence of interference fringes reveals the existence of a microlayer at the base of a growing bubble surrounding the central dry area.

2.2.3. Infrared thermometry

Boiling and condensation are examples of multiphase flows with phase change, in which determining heat transfer and local temperature distributions are important. Infrared thermometry can be used to quantify local temperature distributions (Meola and Carlomagno, 2004), or to visualize the distribution of liquid and gas phases on a surface, enabling identification of the triple contact line, using a technique called DEtection of Phase by Infrared Thermometry (DEPIcT) (Kim and Buongiorno, 2011). Once the temperature on a surface has been assessed, inverse numerical techniques can be used to derive the local heat flux, which is key to understand and model two-phase heat transfer. Given the relatively fast evolution of vapor-liquid flow phenomena, high-speed infrared cameras are required for most studies. Theofanous et al. (Theofanous et al., 2002) were the first to efficiently use

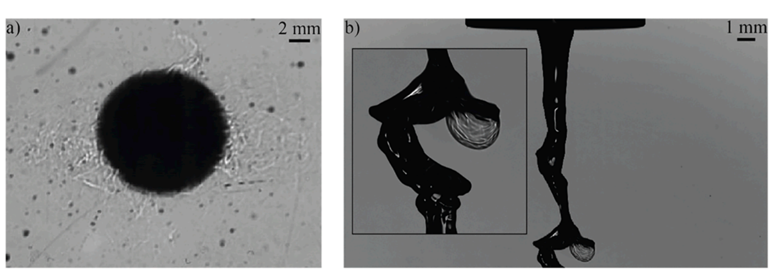

Fig. 1. (a) Shadowgraphy of a freely moving ice sphere melting in a turbulent water flow. The low-temperature meltwater plumes are highlighted since shadowgraphy measures the spatial second derivative of the medium optical index. The setup includes a parallel beam traversing the flow which is focused on the camera sensor (Machicoane et al., 2013); (b) Backlit imaging of the exit of a two-fluid coaxial atomizer. A very small depth of field (aperture F/2) combined with high spatial resolution provides a very sharp gradient at the gas-liquid interface and results in quasi-2D measurements of liquid presence.

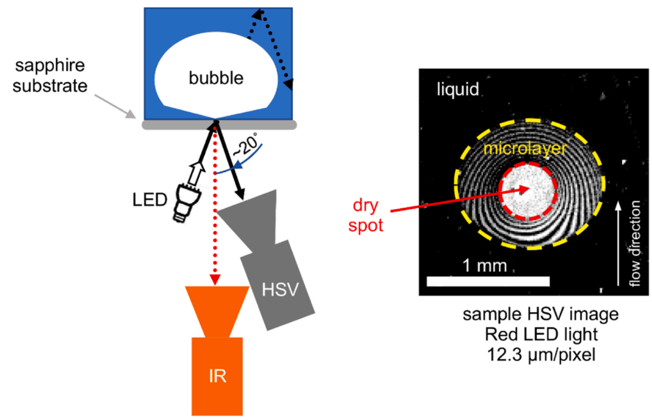

Fig. 2. Schematic of the optical setup used for phase and surface temperature detection (left) and a sample of the acquired image (right) (Reproduced from (Kossolapov et al., 2021)).

high-speed IR imaging to investigate temperature distributions on a boiling surface. When using high-speed IR measurements, reflections of background radiation may influence the results and must be accurately quantified (Sielaff et al., 2019).

IR thermometry may also be used to directly detect the temperature of a liquid interface like a sessile drop. Although the liquid surface should ideally be as close as possible to a black opaque surface, and no liquid presents those ideal characteristics, the effects of surface reflection and semi-transparency of the liquid surface can be quantified to enable characterizing the thermal motion inside a sessile drop (Brutin et al., 2011).

Finally, a combination of infrared and visible light imaging can be employed to simultaneously detect phase and measure temperature distributions over a boiling surface, by using a coating transparent to visible light and opaque to IR (Kossolapov et al., 2021), as shown in Fig. 2.

2.3. *Laser-based*

2.3.1. *Holography*

Holography is inherently a three-dimensional measurement that captures the phase and amplitude of the light diffracted by all objects present along a beam path (Katz and Sheng, 2010). In digital in-line holography, a camera is used to record the diffracted waves from a collimated incoming beam. The setup is typically simpler than most other three-dimensional imaging techniques as it only requires a moderate power laser and one camera. However, the technique is limited by the volume fraction of the dispersed phase that can be tracked. The collimated nature of the beam, which limits depth biases, offers the possibility to accurately measure the size of the imaged objects, but this also makes the positioning of objects along the beam direction less accurate than in the transverse direction. The accuracy of the position along the beam direction can be increased by using inverse reconstruction methods, allowing even objects out of the camera depth-of-field range to be detected at the expense of increased computational cost (Seifi et al., 2013; Soulez et al., 2007).

Holography is well-suited for measuring dispersed multiphase flows with small inclusions and undergoing phase change. It enables particle sizing and tracking (Méès et al., 2020), with recent developments encompassing tomographic velocimetry measurements (Gao and Katz, 2018).

2.3.2. *Particle image velocimetry and particle tracking velocimetry*

Particle Image Velocimetry (PIV) and Particle Tracking Velocimetry (PTV) rely on light scattering by particles to measure the continuous carrier and discrete inclusion velocities. To simultaneously measure the velocity of all phases, phase discrimination is required in the images acquired with high resolution cameras. The locations of the centroids of the particles from each independent phase can be then tracked using a particle tracking algorithm (Clark et al., 2019; Ouellette et al., 2006; Zhang et al., 2008), or PIV cross-correlation algorithms can be applied to the images with flow tracers to obtain the continuous phase velocity field.

Diverse methods have been proposed for phase discrimination, including digital separation using image processing algorithms (Hassan et al., 1992; Honkanen and Nobach, 2005; Khalitov and Longmire, 2002; Kiger and Pan, 2000; Li et al., 2021; Oakley et al., 1997), and optical separation during data collection using wavelength discrimination in dual camera systems (Kosiwczuk et al., 2005, Poelma et al., 2006). Correlation peak discrimination is also possible when there is a significant velocity difference between phases (Delnoij et al., 1999; Rottenkolber et al., 2002). The choice of approach for phase separation is highly dependent on the specific characteristics of the multiphase flow system, with each digital and optical separation presenting advantages and disadvantages which must be considered in a case-by-case basis (Ergin, 2017; Li et al., 2021; Poelma et al., 2006). Most recently, convolutional neural networks have been proposed for phase discrimination, enhancing image processing based methods (Vennemann and Rösgen, 2020; Wang et al., 2022b). In addition to supporting phase discrimination, machine learning (ML) approaches are also being proposed to optimize 3D PTV reconstructions from tomographic measurements (Zhang et al., 2024) and to reconstruct missing data in PIV and PTV measurements (Morimoto et al., 2021; Vlasenko et al., 2015).

There is potential for major improvements in measurement quality, and major decreases in uncertainty and error bounds for the carrier flow velocity and turbulence statistics in close proximity to the dispersed phase particles. Measurements near phase interfaces are of particular interest in turbulent multiphase flows and are generally challenged by particle scattering (Knowles and Kiger, 2012; Martin and García, 2009; Poelma et al., 2006; Seol et al., 2007; Tanaka and Eaton, 2010).

2.3.3. *Phase doppler particle analysis*

The use of Phase Doppler Particle Analysis (PDPA) in dispersed multiphase flows was pioneered by Bachalo (Bachalo, 1994; Bachalo and Houser, 1984; Sankar et al., 1991) and commercialized under different trademarks. It uses the same principle as Laser Doppler Anemometry (LDA), in which 1, 2, or 3 components of the velocity of a scatterer are obtained as it crosses the probe volume (the region of the flow in which the 2, 4, or 6 laser beams of different wavelengths cross) by measuring the Doppler shift in the scattered light. In addition, by placing three photodetectors at slightly different angles at the receiver end, PDPA also measures the phase difference of the scattered light between two pairs of detectors, from which the diameter of the inclusion can be computed from Mie theory, assuming the inclusions are spherical and larger than the light wavelengths.

PDPA is routinely used in dilute bubbly and particulate flows (volume fraction below 10^{-3}, and diameters below 1 mm), and in liquid-gas flows. Since its development, it has become the workhorse for measurements in the dilute region of sprays (Aliseda et al., 2008; Bachalo, 2000; Lasheras et al., 1998; Varga et al., 2003). Tracking the number and velocity of particles in different class sizes can be used to determine the birth, growth, and death of particles of different sizes. These statistical measurements can only be interpreted spatially if the flow is statistically stationary, as the measurements are conducted at a point (small probe volume) as a function of time.

The versatility and reliability of LDA and PDPA have been exploited to fully characterize diverse dilute multiphase flows, including isotropic homogeneous turbulence (Aliseda et al., 2002; Bateson and Aliseda, 2012; Ferran et al., 2023; Mora et al., 2021), free-shear flows (Hishida et al., 1992; Travis et al., 2022), and wall bounded flows (Aliseda and Lasheras, 2006; Felton and Loth, 2002; Kulick et al., 1994; Rogers and Eaton, 1991). One of the limitations of PDPA is that it cannot accurately measure the signal from all particles that cross the probe volume, although if signal rejection is not biased against specific class sizes the diameter distribution is accurately captured (Black and McQuay, 2001). Moreover, with adequate post-processing, the volume flux of the dispersed phase through the probe volume can be reconstructed, effectively filling in those particles whose signal is filtered out (Corcoran et al., 2000). The volume fraction of the dispersed phase can also be quantified when assumptions about the carrier phase velocity can be made, for example that the velocity of the smallest size particles is the same as the local instantaneous carrier flow velocity (Bachalo, 1994; Ferran et al., 2023; Huck et al., 2022; Rácz et al., 2022; Sankar et al., 1991), the volume fraction of the dispersed phase can be quantified (Roisman and Tropea, 2001).

Another drawback of PDPA measurements is that number densities are often underestimated for the smallest particles, typically those between 1.5-10 microns in diameter (Sankar et al., 1991), depending on the wavelength and laser intensity/transmitting-receiving optics (Knop et al., 2021; Qiu and Sommerfeld, 1992; Qiu et al., 2001).

2.4. Soft-field measurements

Soft-field measurement techniques are those in which the electric or magnetic sensing field is strongly influenced by the properties of the medium being measured and their spatial distribution (Abdul Wahab et al., 2015). Depending on how the waves interact with the surrounding media, some techniques can be classified as either soft-field or hard-field (described in Section 2.5). Because the measurement quantity is affected by the entire medium, the reconstruction algorithms for soft-field tomography are complex, with reconstruction outputs that can be very sensitive to noise and small measurement variations, and that involve iteration and error minimization techniques (Cui et al., 2016; Fessler, 2020; Yorkey et al., 1987).

2.4.1. Electrical tomography

The measurement principles of the resistance, capacitance, or impedance probe techniques discussed in Section 2.1.3 have been extended to field measurements using tomographic reconstructions of resistance, capacitance, or impedance measurements from detectors arranged in the periphery of the multiphase flow system (Cui et al., 2021; Rasel et al., 2022; Yao and Takei, 2017). Fig. 3a shows a schematic diagram of a simple electrical impedance tomography (EIT) electrode arrangement for collecting impedance data. Here the impedance between pairs of electrodes is measured by applying a constant current input and output, in this case at two electrodes. The resulting voltage at all electrodes is recorded, producing one “projection”. With N electrodes, there are $R_N = N(N-1)/2$ linearly independent projections. Practical implementation of EIT electrode arrays can be more complex, incorporating a variety of electrode geometries (e.g., circular, planar, spiral) along with “guard” electrodes that can be used to manage current flows outside and at the boundary of the measurement domain. Similar arrangements can be used for electrical resistance tomography (ERT) or electrical capacitance tomography (ECT).

Fig. 3b presents a typical EIT reconstructed image, which illustrates how different reconstruction methods can yield varying impedance distributions in the domain. Challenges to the implementation of EIT rest primarily with the fact that there usually is not a unique solution to the impedance distribution given a finite number of measured projections. This results from the fact that the current lines within the domain are significantly altered by the phase distribution itself; hence, the “soft field” designation. Additional *a priori* constraints on the impedance field are often imposed to force the candidate reconstruction toward a desired phase topology. Some EIT systems that are meant to examine contrast in capacitance can have significant current flows not just within the multiphase flow but also within the flow container itself. In these cases, the impedance of the flow and the container must be part of the reconstruction.

Other practical challenges with the implementation of EIT include the nature of the data collection itself, limitations in the electrode size and geometry, and current leakage. Even with these challenges, EIT (ECT or ERT) has proven to be a relatively low-cost method to non-invasively interrogate the field properties of a multiphase flow with high temporal resolution, with particularly successful implementations for

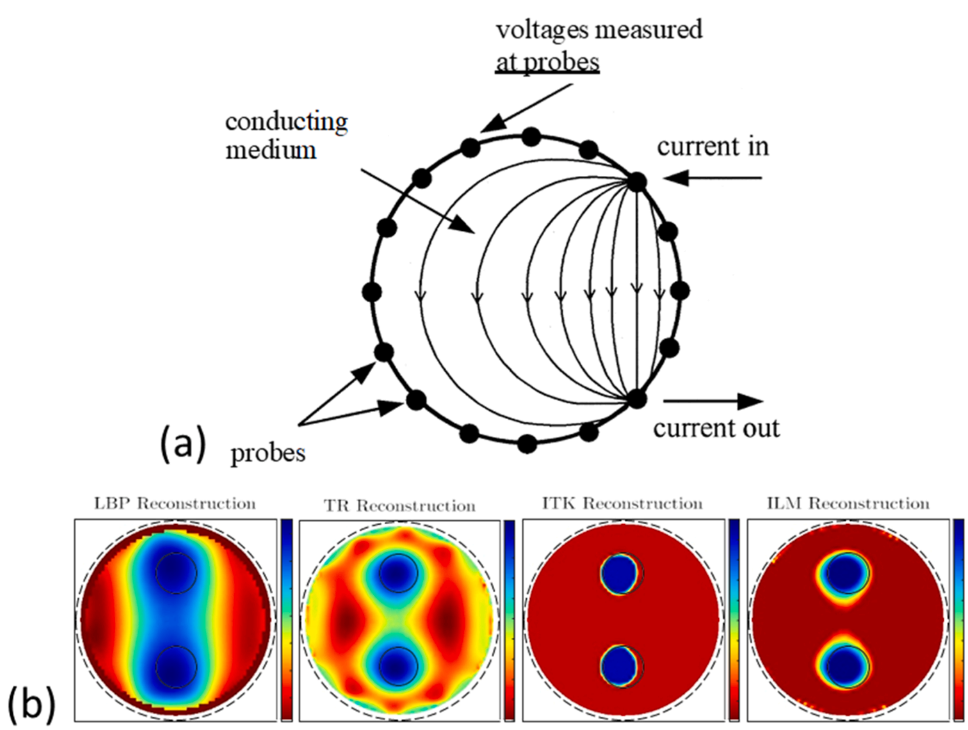

Fig. 3. (a) Schematic diagram of a simple EIT electrode geometry applied to circular domain (Reproduced from (George et al., 2000b)). (b) An example EIT reconstruction of air bubbles dispersed in oil using four different reconstruction methods (Reproduced from (Rasel et al., 2022)).

process control (Tapp et al., 2003).

2.4.2. Magnetic resonance imaging

Magnetic resonance imaging (MRI) techniques enable measurements in optically opaque multiphase flows, including combinations of solids, liquids, and gases. No constraint is imposed on the flow geometry imaged, but the flow apparatus must fit within a clinical or research-grade MRI scanner, and it must be MRI compatible (non-ferromagnetic). MRI is rooted in nuclear magnetic resonance (NRM), to which Lauterbur (Lauterbur, 1973) and Mansfield (Mansfield, 1977) added the ability of spatial distinctions by using magnetic field gradients superposed to the main magnetic field. A pulse radiofrequency excitation creates a net magnetization that disturbs the spin of the atomic nuclei (generally hydrogen protons in water) away from alignment with the magnetic field. As spins precess post-excitation while re-aligning with the main field, the precessing magnetization produces an induced electric current, the signal measured at antennas in an RF coil. By selectively varying the magnetic field gradients and the RF excitation frequencies across multiple transmit/receive cycles, it is possible to reconstruct three-dimensional images of the spatial distribution of distinct phases as well as mean velocity fields.

The spatial resolution is generally limited by the measurement signal-to-noise ratio and scan time. Resolutions as small as several microns can be achieved with state-of-the-art high-field scanners (e.g., 9.4T), while submillimeter spatial resolution is most common with 3T scanners. The scan time depends on the dimensionality and spatial resolution of the output, but also on the substances imaged and imaging sequence, ranging from milliseconds for 1D imaging to minutes for 3D imagining with high spatial resolution. Due to its versatility in terms of measurement quantities, MRI extends to many fields beyond its main thrust in medical and biomedical applications. Fukushima (Fukushima, 1999) provides an early review of the use of MRI with a focus on velocity and concentration profiles in a wide variety of multiphase flows. Many reviews have followed (Clarke et al., 2023; Elkins and Alley, 2007; Gladden and Sederman, 2017; Mantle and Sederman, 2003; Stannarius, 2017). Reference books (Brown et al., 2014; Callaghan, 1993) are available that provide in depth details on MRI, sequence design, and reconstruction strategies.

Contrast agents in small concentrations are often added in flow experiments to reduce scan times and increase signal strength by decreasing the relaxation times of hydrogen nuclei. The relation between concentration of a contrast agent and signal magnitude has also been exploited to measure turbulent transport of a passive scalar via concentration field measurements (Banko et al., 2020; Benson et al., 2010). Signal magnitude has been largely used in multiphase flows for void fraction measurements in granular media (Stannarius, 2017), moving bubbles (Tayler et al., 2012a), and particles (Borup et al., 2018), as well as to identify cavitation (Adair et al., 2018). The sensitivity of MRI signal to temperature is also widely exploited for thermometry in medical applications (Rieke and Butts Pauly, 2008), and heat transfer experiments (Serial et al., 2023; Zhang et al., 2022).

Many of the works already introduced combine measurements of concentration, temperature, or void fraction with velocimetry. Phase encoding, or phase contrast (PC) imaging (Dumoulin et al., 1989; Pelc et al., 1991a), is the most common method for mean velocity field measurements and has been used in many complex flow configurations (Banko et al., 2015; Bruschewski et al., 2023; Elkins et al., 2003; Grundmann et al., 2012). Time periodic flows can also be measured by using gated scans and distributing the different phase encodes required for spatial localization over successive cycles (Pelc et al., 1991b). This modality, termed PC cine MRI, is commonly used for blood flow (Markl et al., 2003; Markl et al., 2012) and has been applied for measurements in rotating (Hoffman et al., 2020) or pulsatile flows (Benson et al., 2023). Shorter acquisition times are needed in fast moving or unsteady flows, and to some extent they can be achieved with tradeoffs in spatial resolution and signal-to-noise ratio (Elkins and Alley, 2007). Sequences using echo planar imaging (EPI) and multi-shot EPI largely decrease acquisition times to hundreds of milliseconds and have been used in drops and rising bubbles (Amar et al., 2010; Kemper et al., 2021). Acquisition times can also be reduced by non-uniform undersampling using compressed sensing techniques (Fu et al., 2015; Tayler et al., 2012b).

There are several sources of uncertainty in MRI measurements that depend on the scanner (the non-linearity of fields and gradients), the sequences, and also on the multiphase flow under study, with scan parameters that need to be optimized for each experiment (Elkins and Alley, 2007). The velocimetry measurement accuracy has been addressed using statistical measures (Bruschewski et al., 2016) and by comparison to PIV (Elkins et al., 2009; John et al., 2020). The robustness of MRI velocimetry to hardware, sequence, and user defined MRI parameters has been demonstrated in MRI challenges where measurements on the same flow phantom were compared across different groups using different scan manufacturers and sequences (Benson et al., 2023; Benson et al., 2020).

As MRI hardware continues evolving, with medical-grade scanners becoming more easily accessible, and with the increase of affordable low field scanners, the development of tailored MRI techniques has a strong potential in multiphase flows measurements.

2.5. Hard-field measurements

In contrast to soft-field measurement techniques, hard-field techniques measure a property that is independent of the volumetric distribution of the discrete phase. Hard-field measurements are easier to interpret than soft-field measurements because the wave paths are predictable. Examples of hard-field techniques include X-ray, optical, ultrasonic tomography (in relatively dilute multiphase systems), and short-range radar systems.

2.5.1. Acoustic/ultrasound

Contrast in the acoustic properties of the phases in a multiphase flow invite the use of sound waves to interrogate the phase distribution and other properties of the flow. In many cases ultrasound is employed to determine phase boundaries and velocities in the spatially averaged bulk or as 2D or 3D distributions. Recent reviews of these methods are available (Fan and Wang, 2021; Hossein et al., 2021; Poelma, 2016, 2020; Tan et al., 2021).

One modality of ultrasound measurements relies on the Doppler effect, whereby the frequency of a reflected sound wave is increased (or decreased) as the object reflecting the sound is moving toward (or away) from the receiver. Ultrasound waves with frequencies on the order of 1-10 MHz can be transmitted into a flow using either continuous (Continuous Wave Ultrasound Doppler, CWUD) or pulsed (Pulsed Wave Ultrasound Doppler, PWUD) waves. Ultrasound that reflects off particulates or larger phase boundaries in a moving fluid will undergo a Doppler shift, and measurement of the reflected signal will yield the phase velocity. Ultrasonic Doppler methods are quite amenable to homogeneous dispersed flows, where the path of sound propagation and reflection are relatively well understood *a priori*. They may also be used when there are strong variations in the phase topology, such as in the cases of stratified, annular, or bubbly flow (Figueiredo et al., 2016). The interaction of the sound wave with compressible phases of the flow can result in changes to the bulk sound speed and/or acoustic resonance. In these cases, interpretation of the acoustic return is more challenging, and may require extensive calibration with known flow topologies along with sophisticated data processing.

It is also possible to use ultrasound for flow imaging (Poelma, 2016). These methods use technology that has been developed for medical ultrasonic imaging, allowing for whole field resolution of the phases of the flow, or even measurements of phase velocities with time resolved methods, named Ultrasound Imaging Velocimetry or echo-Particle Imaging Velocimetry. Efforts are underway to adapt and optimize medical imaging systems for multiphase flows, which will likely involve new specific signal processing algorithms.

Finally, Hossein et al. (Hossein et al., 2021) reviewed how sound emitted from the multiphase flow itself can be used as a diagnostic tool. Phase interactions within the bulk of the flow and at the flow boundary can create sound across a range of frequencies, including audible and ultrasonic, which can be correlated to the flow parameters of interest, such as flow speed, phase fraction, or topology.

2.5.2. Millimeter wave

Millimeter waves (MMW) are radio frequency waves in the 30-300 GHz frequency range, with wavelengths on the order of 1 to 10 mm. MMW interferometry has been conventionally exploited for electron density measurements in plasma systems (Hartfuss et al., 1997), and only in the last decade the use of MMW has extended to medical imaging (Topfer and Oberhammer, 2015; Wang et al., 2014), and short-range sensing in autonomous vehicles (Polese et al., 2023).

Techniques for multiphase flows have been more common in the low microwave frequency range, based on measurements of transmitted or reflected waves whose amplitude and phase vary with the bulk complex dielectric constants of the mixture. One of the first microwave sensors was developed for oil measurements (Ashton et al., 1994), and it is common in industrial monitoring (Nyfors, 2000). Microwave techniques are used for the identification and concentration of specific ingredients in liquid mixtures (Bo and Nyfors, 2002; Gennarelli et al., 2013), and oil and moisture content in porous materials and emulsions (Aggarwal and Johnston, 1986; Pal, 1994). Microwaves can also be used as a soft-field technique for microwave tomographic imaging (MTW) (Mallach et al., 2017; Wu, 2015)

Increasing the frequency into the MMW band allows for better spatial and temporal resolution, and for compact hardware with multiple small antennas, but penetration depths are reduced. Dispersed multiphase flows with air as the dominant phase and dielectric materials with low tangent losses are ideal candidates for MMW sensing. They have been used to measure the liquid, vapor, ice, and mixture composition of clouds, the size and shape of drops or ice crystals (Hogan et al., 2000; Oue et al., 2015), and their velocity and atmospheric turbulence profiles (Kollias et al., 2001). Reviews on MMW atmospheric radars are available (Kollias et al., 2016; Kollias et al., 2007). Similar techniques have been used in volcanology to measure ash size distributions and velocities using pulsed-Doppler radars or frequency modulated continuous wave (FMCW) radars (Bryan et al., 2017; Hort and Scharff, 2016). CW Doppler radars have also been proposed to measure ejecta velocities generated by the impingement of rocket plumes on a planetary surface (Kemmerer et al., 2023).

FMCW MMW radars can be used to measure the volume fraction in dispersed multiphase flows. One of the first demonstrations used a custom-made radar system to measure volume loading in a pneumatically conveyed system carrying 30 μm wheat flour particles (Baer et al., 2014). Recently, using a compact and inexpensive Texas Instrument FMCW MMW radar and a passive reflector, interferometry was used to measure the path integrated concentration of 103 μm glass microspheres in a rapidly evolving cloud with 50 μs temporal resolution (Rasmont et al., 2023). With FMCW radars now available as off-the-shelf integrated systems for automotive applications, MMW interferometry emerges as a low-cost and low-complexity technique to measure path-integrated number or volume concentration in optically opaque regimes. The technique has been recently validated and its measurement accuracy evaluated for different calibration methodologies (Rasmont et al., 2025b). By extending the setup to a multi-path measurement system, as shown in Fig. 4, using exclusively one radar integrating emit and receive antennas and multiple passive reflectors, MMW interferometry has been extended to a tomographic imaging system providing high speed measurements of particle concentration distributions (Rasmont et al., 2024). Local volume concentrations up to 3% were measured.

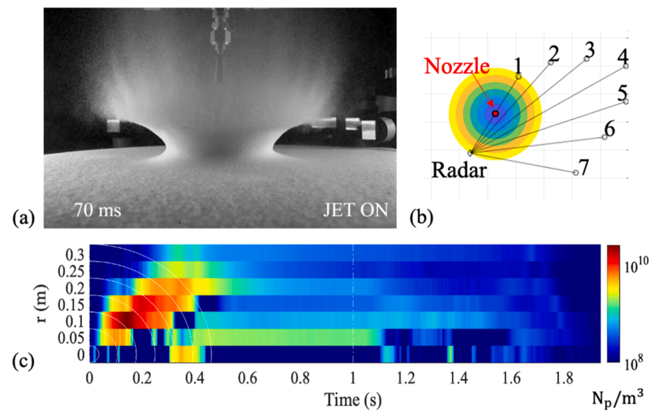

Fig. 4. Particle concentration measurement via MMW tomography during supersonic jet impingement on a granular surface, experiment described in (Rasmont et al., 2024). (a) Instantaneous snapshot from high-speed camera; (b) radar-reflectors arrangement; and (c) radial distribution of particle concentration at a plane above the surface sampled at 10 kHz during a 1 sec flow-on experiment.

The spatial resolution of MMW interferometry is limited to centimeters when passive reflectors and simple off-the-shelf radars with a reduced number of antennas are used. Future developments exploiting phase array radars and active reflectors offer promising opportunities for improved spatial resolutions. The same system used for volume fraction measurements also provides velocimetry using the Doppler-shift return.

2.5.3. X-ray imaging

X-ray imaging is performed by placing an X-ray source behind a sample such that a beam is shot through it to be imaged by a detector. X-rays, unlike visible light, benefit from weak scattering by gas-liquid interfaces and have been shown to be among the best candidates for probing optically dense multiphase flows due to its penetrative nature and high energy (Aliseda and Heindel, 2021; Heindel, 2024). In most X-ray imaging systems, the X-ray beam is absorbed by a scintillator crystal that re-emits visible light proportional to the X-ray intensity and this light is then captured by a camera. X-rays are generally safer than γ-rays because the sources only emit X-rays when they are powered and their energy can be controlled by varying the input voltage (Chaouki et al., 1997; Toye et al., 1996). X-rays also have better available detectors and smaller spot sizes than γ-rays, which provides better spatial resolution (Heindel, 2011).

At the lab scale, X-ray imaging has been primarily developed to perform 3D tomographic reconstructions of the sample composition. Tomographic measurements require rotating the object of interest; for multiphase flows, this could lead to non-negligible Coriolis effects and non-trivial mechanical issues. This difficulty may be overcome by using multiple sources and detectors or by spinning the X-ray equipment around the experiment (Heindel, 2024). However, X-ray imaging with a single source and detector, called radiography, can still give access to time-resolved projected mass distribution maps. Many developments in lab-scale X-ray imaging techniques adapted to multiphase flows have emerged over the past few decades (Heindel, 2011, 2018; Heindel, 2024). In the context of cavitation for example, 2D measurements of the projected time-average void fraction with high temporal resolution have been conducted using tube-source X-rays (Ganesh et al., 2016; Maurice et al., 2021). Many other examples of multiphase flow imaging using X-rays are summarized in a recent review (Heindel, 2024).

Beyond quantitative local time-average mass measurements, X-ray imaging has been used for X-ray particle tracking velocimetry (XPTV) in fluidized beds (Chen et al., 2019a, b) and granular mixers (Kingston et al., 2015; Nadeem et al., 2023). New micro-focus X-ray tubes with a liquid metal jet anode X-ray have recently been used to track micron-sized particles at kHz imaging speeds (Parker et al., 2024). Additionally, using only 2D time-resolved radiography and spheres of known size, one can obtain the 3D position and perform tracking with only one projection when using a diverging X-ray cone beam (Stamati et al., 2023).

High-speed synchrotron X-ray imaging has also been used for multiphase flow studies (Heindel, 2018; Kastengren et al., 2023; Kastengren and Powell, 2014). Ideal multiphase flows include cavitation (Biasiori-Poulanges et al., 2023; Khlifa et al., 2017) and spray formation (Bothell et al., 2022; Li et al., 2017; Machicoane et al., 2019; Tolfts et al., 2024) because of the required small spatial and temporal scales as well as the optically dense nature of these turbulent multiphase flows.

2.5.4. γ-rays

In contrast to X-rays, γ-rays have higher photon energies that provide better penetration through dense-walled containment vessels. X-rays also require external cooling systems and a stable high voltage power supply, whereas γ-rays are provided by isotopic sources, which are insensitive to thermal and electrical fluctuations. These factors make γ-ray densitometry a workhorse for industrial tomography in the chemical and process industries (Bieberle et al., 2013; de Mesquita et al., 2016; Johansen, 2015).

Several groups have used γ-rays for projected void fraction or density measures in various multiphase flows. Single projection measurements have been used to quantify void fraction in a variety of systems, including industrial-sized bubble columns with stainless steel walls (Jin et al., 2005), pilot scale packed beds with gas-liquid up flow (Toukan et al., 2017), and a 440 mm diameter column filled with structured packing and a volatile fluid (Hoffmann and Kögl, 2017). Chord-average void fractions have also been reported for concurrent downflow bubble columns (Hernandez-Alvarado et al., 2017).

Rotating the γ-ray source and detector array (Shaikh et al., 2023) or arranging multiple sources and detectors around the flow of interest (Yan et al., 2021) allows for the use of reconstruction techniques to visualize the time-average void fraction across a given plane. These γ-ray tomographic techniques have been applied to bubble columns (de Mesquita et al., 2016), bubble columns with internals (Sultan et al., 2018), gas-liquid-solid slurry bubble columns (George et al., 2001; Shaikh et al., 2021), and an aerated stirred-tank reactor (Khopkar et al., 2005).

Two different γ-ray sources with different energies can also be used and have the advantage of providing dual energy measurements that can be applied to three-phase systems. A dual-source γ-ray computed tomography system has been used to visualize and quantify void fraction in a pebble bed reactor (Al Falahi and Al-Dahhan, 2016), bubble column (Sultan et al., 2018), spouted bed (Al-Juwaya et al., 2017), and fluidized bed (Efhaima and Al-Dahhan, 2015).

3. Outlook

3.1. New developments

Tackling detailed experimental multiphase flow studies typically requires the combination of several experimental techniques for measuring the same quantity of interest but in different regimes, or different quantities of interest. Spray measurements are one example where several techniques exist to measure droplet size, each preferred depending on the region of the spray and atomization parameters. Methods may be combined to fully characterize a broad droplet size population, accurately measuring droplet diameter using Phase Doppler Interferometry and direct backlit imaging (Huck et al., 2022), and quantifying the 3D volume of larger lumps of fluids using backlit imaging from several projections (Masuk et al., 2019). In addition, droplet velocities can be simultaneously measured with LDA and high-speed imaging, with other techniques needed for measurements of the carrier phase. Some of these measurements can now be performed simultaneously thanks to more compact and robust systems as technologies mature.

In general, combining diagnostics for multi-parameter measurements is challenged by the complexity of the different measurement techniques and their setups, incompatibilities on their requirements, and crosstalk between systems. Recent reviews have specifically focused on the combination of established measurement techniques for simultaneous measurements in single and multiphase flows (Hao et al., 2023; Li et al., 2023).

New developments in advanced techniques for probing multiphase flows will continue to strengthen multi-technique approaches, with new strategies for synchronized measurements using different sensing principles while avoiding signal interference. New hardware and software advances push the limits of measurement resolution and signal-to-noise ratio and increase accessibility to advanced dedicated equipment. One recent example of a multi-technique approach enabled by highly specialized testing facilities with high potential to dense multiphase flows is the leveraging of simultaneous X-ray and neutron imaging to measure the evolution of moisture migration in porous media while reconstructing its changing 3D geometry (Sleiman et al., 2021).

In the area of dispersed multiphase flows, advanced multi-antenna technology and compact radar systems present great potential and are now widely accessible at low cost; their rise driven by increasing demand for communication bandwidth and short-range autonomous vehicle sensing. The small size of MMW components allows combining multiple arrays of antennas in compact configurations, with techniques like Multiple-Input Multiple Output (MIMO) and beam forming (Heath et al., 2016; Sun et al., 2014) boosting the resolution and dynamic range while enabling simultaneous measurements of velocity and concentration from different properties of the recorded signal. The use of active reflectors or tags, selectively modulating the waves, also increases the measurement range and resolution (Soltanaghaei et al., 2021), and limits crosstalk, at the expense of added complexity. The main strengths of MMW radars for dispersed multiphase flows are their high temporal resolution, and their capability to measure in a range of volume loadings which is usually restricted to optical techniques due to excessive attenuation and being too dilute for X-ray imaging. In addition, they are easy to integrate with other diagnostics without signal interference. MMW systems can be incorporated into high-speed and X-ray imaging setups for the study of time-varying dispersed multiphase flows which undergo a wide range of volume loading conditions, as is the case of a gas plume interacting with a granular surface (Rasmont et al., 2025a). The increasing accessibility to lab-scale X-ray imaging, and advanced micro-focus X-ray tubes (Parker et al., 2024) also facilitate multi-technique approaches.

Hardware developments are key to advanced diagnostics and improved spatial and temporal resolution. Sensors continue to shrink, becoming less intrusive in flow measurements, and higher speed lasers, electronics, and camera sensors, with increasing image sizes and sensibility, enable faster acquisitions and time-resolved measurements. Improved sensors and cameras are dramatically increasing the amount of data that can be collected, requiring new data analysis and data management methods. As larger amounts of experimental multiphase flow data become available, artificial intelligence (AI) and data-driven ML approaches are increasingly being used for classification, pattern recognition, model discovery, and development of closure models (Al-Naser et al., 2016; Basha et al., 2024; Quintino et al., 2021; Zhu et al., 2022). Neural networks are well suited and widely exploited for image segmentation and data enhancement (Foster et al., 2025) and have a large potential in dispersed multiphase flows to facilitate the detection and characterization of the dispersed phase (Hessenkemper et al., 2022). ML techniques are also being exploited for faster and more accurate flow field and trajectory reconstructions from PIV and PTV measurements, respectively (Tirelli et al., 2023; Wang et al., 2022a), and data-driven ML has also been used to develop bubble and droplet size distribution predictions based on measured flow conditions (Basha et al., 2024; Zhu et al., 2022).

Experimental data are key to drive the discovery of physical mechanisms, and to develop and validate models, but it is not possible to measure all the desired quantities of interest in a dispersed multiphase flow experiment. Data assimilation and ML techniques combining large volumes of sparse data from different diagnostics with numerical simulations present a promising opportunity to reconstruct missing experimental data (Zhao et al., 2024) and to develop physics-constrained models with predictive capabilities.

The tremendous advances in numerical simulations of multiphase flows, and the increase in computational power over the past decades, now enable high-fidelity simulations of regimes comparable to laboratory scale experiments in many cases. Joint experimental-numerical studies remain a necessary avenue to advance multiphase flow science and technology in a manner that is inaccessible to experimental analysis or numerical simulations alone. Simulations provide the three-dimensional time-resolved information necessary to understand the flow physics (Balachandar, 2024; Elghobashi, 2019; Fox, 2012; Subramaniam, 2020; Subramaniam and Balachandar, 2022; Tryggvason et al., 2011), while experiments showcase the ground truth required to identify missing physics in the equations and validate physics-based models. Only the synergistic coupling of both approaches can fully unravel complex phenomena. A few recent examples of the power of joint experimental-numerical studies include: (i) the instability mechanism in the primary breakup region of planar coflowing sheets (Fuster et al., 2013), (ii) the development of a phenomenological equation to predict the velocity of the jets formed by bubble bursting contributing to aerosol formation above the ocean (Deike et al., 2018), (iii) the development length and particle-particle collision models required in dilute turbulent particle-laden flow simulations (Esmaily et al., 2020), and (iv) the importance of contact line dynamics when modeling the exit region of an airblast atomizer (Vu et al., 2023). Careful data preprocessing must be executed when performing one-to-one comparisons to account for real effects on the diagnostic techniques (e.g., laser thickness, distortions, implicit biases, etc.) and the implemented computational model (e.g., numerical method, convergence, grid resolution, etc.).

It is important to remember that there is no experimental technique or combination that can simultaneously measure the three-dimensional properties of the dispersed and continuous phases in a time-resolved manner. Likewise, there is rarely a situation of scientific or practical interest in which a numerical simulation of a dispersed multiphase flow, especially in a turbulent carrier phase, can be considered a true Direct Numerical Simulation without any modeling involved. Thus, experiments are critical in guiding and validating the use of models for dispersed/continuous phase flow interactions. At the same time, simulations can provide a wealth of spatial and temporal information that is simply not accessible in experiments.

3.2. Future research opportunities

Dispersed multiphase flows encompass a wide range of physical phenomena important to diverse applications with large societal and technological impact. A few selected research directions of growing scientific interest, with strong potential for major advances, are briefly introduced here and include areas such as medical treatment, environmental preservation, industrial processes, high-speed or reactive flows, and space exploration.

Dispersed multiphase flows are intrinsic to human body fluids, medical applications, and disease transmission. The importance of fundamental knowledge on droplet dispersion and evaporation in a turbulent flow was irrefutably evident during the COVID-19 pandemic, when it became clear that airborne transmission of pathogen-laden droplets and particles was an important contributor to rapid disease spread (Balachandar et al., 2020; Bourouiba, 2021). Additionally, targeting inhaled drug-aerosol delivery to predetermined lung areas requires knowledge of particle transport and deposition in the complex human airways (Banko et al., 2015; Kleinstreuer and Zhang, 2010). Active research is being focused on micro-particle or droplet encapsulated drugs delivered into the bloodstream, which serve as cavitation nuclei with targeted drug release then triggered by ultrasounds (Stride and Coussios, 2019). Ultrasound techniques, now commonly used in bubbly flows, emerged as a biomedical imaging diagnostic that later found is way as a therapeutic tool, with acoustic cavitation used to deposit heat deep within the body for ablation of tumor cells, and for enhanced mass transport across inaccessible interfaces such as the blood-brain barrier (Brennen, 2015; Coussios and Roy, 2008; Yuan et al., 2015).

Bubble and droplet-laden flows undergoing phase change (e.g., evaporation, dissolution, melting, freezing) involve momentum and energy coupling between phases, that often occur over a wide range of length and time scales within a carrier turbulent flow (Ni, 2024). In addition to a myriad of industrial processes, dispersed droplet and particle laden flows with phase change, or mass and energy exchange, are intrinsic to many large-scale environmental flows that affect our ecosystem (Dauxois et al., 2021). An example is the bubble-mediated air–sea mass exchange and gas spray production, which control the fluxes of gases, moisture, and sea salt that regulate the ocean–atmosphere interaction from local to global scales (Deike, 2022).

Another example of the importance of particle-laden flows with mass transport is the attempts to slow global warming by carbon sequestration, from the atmosphere or flue gases, by using microparticles with liquid carbonate cores and silicone shells to increase the surface area, and thus the carbon dioxide absorption rate (Vericella et al., 2015). Droplet breakup and vaporization are also of upmost importance in compressible flow regimes, in which shock-driven breakup creates additional hydrodynamic instabilities. The compressible multiphase flow regime is key to liquid-fueled detonation (Young et al., 2025), and to supersonic flight, with small drops becoming impactors that are first processed by a bow shock prior to their hypervelocity impact onto the vehicle (Dworzanczyk et al., 2025).

With increasing interest in space exploration, prolonged human activity in microgravity conditions, and efforts to sustained operation on other planetary and celestial bodies, like Mars or the Moon, there is an increasing need to advance our understanding of multiphase flow processes under varying gravitational effects and reduced pressure environments. Many multiphase flow phenomena are noticeably affected by gravitational acceleration, including phase separation, bubble dynamics and detachment, and in general the dynamics of the dispersed phase with non-negligible mass. Experiments at varying gravitational acceleration serve to assess theoretical and empirical models, and to evaluate the performance of devices such as propellant storage, two-phase heat exchangers, or regenerative life support systems. Phase separation, boiling and critical heat flux, instabilities and transient conditions are some of the priority multiphase flow research areas for safe in-space operations (Garivalis and Di Marco, 2022; Konishi and Mudawar, 2015; Nejati et al., 2020; Ulucakli and Merte, 1990; Zhao and Rezkallah, 1993).

One interesting effect in reduced gravity is captured by the Bond number, which scales the size of the experiment with the capillary length. The capillary length increases with decreasing gravity (inversely proportional to the square root of gravity), therefore "small" capillaries become "large" in microgravity, allowing more detailed diagnostics of local phenomena (Di Marco et al., 2009). The International Space Station can be used to study gravity effects (Sielaff et al., 2022). On Earth, gravity effects can be studied in small scale experiments in a centrifuge, drop tower, or parabolic flight (Brendel et al., 2023). The dynamics of particles at high Knudsen numbers become important at the very low pressures of the Moon during the propulsive descent of a lander (Cuesta et al., 2025; Rahimi et al., 2020). Lifted regolith particles not only prevent surface visibility, as documented during the Apollo Missions and the recent Firefly Blue Gosht lunar descent, but also endanger the vehicle and nearby infrastructure, with similar and unknown risks during Martian descents. Electrostatic charging, and electrical storms on Mars (Di Renzo and Urzay, 2018) are other fascinating particle-laden flow phenomena to be unraveled.

Finally, advanced laser diagnostics for regimes involving high temperature and reactive multiphase flows, relevant to hypersonics and combustion environments, have seen enormous progress in the last decades, with still much potential to further develop experimental diagnostics for quantitative measurements. The continuous progress towards compact and broadly accessible hardware that can be used in harsh environments, in laboratory or field experiments, is well posed to bring fast-paced advances on all aspects of dispersed multiphase flows. All these challenges and opportunities make it exciting to be a multiphase flow experimentalist.

4. Conclusions

Dispersed multiphase flows are ubiquitous and involve a wide range of multi-physics phenomena. Continuous advancements in experimental methods are needed to better understand the underlying physics of dispersed multiphase flows, and to guide and validate models that can be used for system design and prediction. Despite the experimental complexities introduced by the presence of the dispersed phase when compared to single phase flow experiments, several methods are currently available that provide many of the desired quantities of interest. Experimental techniques reviewed in this work include invasive probes, optical and laser-based imaging, and soft- and hard-field electromagnetic sensing methods with tomographic capabilities for three-dimensional measurements. Hardware developments continuously push the limits of existing techniques in terms of temporal and spatial resolution and offer opportunities for tailoring selected hardware that were originally developed for other applications (i.e., medical imaging, telecommunications, or materials inspection) to multiphase flows measurements. Dispersed multiphase flows with high volume loadings of the dispersed phase, and those involving high-temperature, high-speed, and reactive environments, still pose major challenges to experimental measurements, with many opportunities for researchers to make their mark in experimental multiphase flows.

CRediT authorship contribution statement

Laura Villafañe: Writing – review & editing, Writing – original draft, Conceptualization. **Alberto Aliseda:** Writing – review & editing, Writing – original draft, Conceptualization. **Steven Ceccio:** Writing – review & editing, Writing – original draft, Conceptualization. **Paolo Di Marco:** Writing – review & editing, Writing – original draft, Conceptualization. **Nathanaël Machicoane:** Writing – review & editing, Writing – original draft, Conceptualization. **Theodore J. Heindel:** Writing – review & editing, Writing – original draft, Project administration, Conceptualization.

Declaration of competing interest

The authors declare that they have no known competing financial interests or personal relationships that could have appeared to influence the work reported in this paper.

Data availability

No data was used for the research described in the article.

References

Abdul Wahab, Y., Abdul Rahim, R., Fazalul Rahiman, M.H., Ridzuan Aw, S., Mohd Yunus, F.R., Goh, C.L., Abdul Rahim, H., Ling, L.P., 2015. Non-invasive process tomography in chemical mixtures – A review. Sens. Actuators B: Chem. 210, 602–617.

Abel, R., Resch, F., 1978. A method for the analysis of hot-film anemometer signals in two-phase flows. Int. J. Multiph. Flow 4 (5-6), 523–533.

Adair, A., Mastikhin, I.V., Newling, B., 2018. Motion-sensitized sprite measurements of hydrodynamic cavitation in fast pipe flow. Magn. Reson. ImAging 49, 71–77.

Aggarwal, S.K., Johnston, R.H., 1986. Oil and water content measurement of sandstone cores using microwave measurement techniques. IEEE Trans. Instrum. Meas. 4, 630–637.

Al-Juwaya, T., Ali, N., Al-Dahhan, M., 2017. Investigation of cross-sectional gas-solid distributions in spouted beds using advanced non-invasive gamma-ray computed tomography (CT). Exp. Therm. Fluid. Sci. 86, 37–53.

Al-Naser, M., Elshafei, M., Al-Sarkhi, A., 2016. Artificial neural network application for multiphase flow patterns detection: A new approach. Journal of Petroleum Science and Engineering 145, 548–564.

Al Falahi, F., Al-Dahhan, M., 2016. Experimental investigation of the pebble bed structure by using gamma ray tomography. Nuclear Engineering and Design 310, 231–246.

Aliseda, A., Cartellier, A., Hainaux, F., Lasheras, J.C., 2002. Effect of preferential concentration on the settling velocity of heavy particles in homogeneous isotropic turbulence. J. Fluid. Mech. 468, 77–105.

Aliseda, A., Heindel, T.J., 2021. X-ray flow visualization in multiphase flows. Annu Rev. Fluid. Mech. 53, 543–567.

Aliseda, A., Hopfinger, E.J., Lasheras, J.C., Kremer, D., Berchielli, A., Connolly, E., 2008. Atomization of viscous and non-newtonian liquids by a coaxial, high-speed gas jet. Experiments and droplet size modeling. Int. J. Multiph. Flow 34 (2), 161–175.

Aliseda, A., Lasheras, J., 2006. Effect of buoyancy on the dynamics of a turbulent boundary layer laden with microbubbles. J. Fluid. Mech. 559, 307–334.

Alonzo, M., Lefebvre, A., Huang, Z., Gluck, S., Cartellier, A., 2023. Doppler optical probe for drop size, velocity, and flux measurements in assisted atomization. Atomization and Sprays 33 (7).

Amar, A., Blümich, B., Casanova, F., 2010. Rapid multiphase flow dynamics mapped by single-shot MRI velocimetry. Chemphyschem. 11 (12), 2630–2638.

Ashton, S., Cutmore, N., Roach, G., Watt, J., Zastawny, H., McEwan, A., 1994. Development and trial of microwave techniques for measurement of multiphase flow of oil, water and gas. In: SPE Asia Pacific Oil and Gas Conference and Exhibition. Melbourne, Australia. SPE. Paper SPE-28814-MS.

Bachalo, W., 1994. Experimental methods in multiphase flows. Int. J. Multiph. Flow 20 (Supplement), 261–295.

Bachalo, W., 2000. Spray diagnostics for the twenty-first century. Atomization and Sprays 10 (3-5), 439–474.

Bachalo, W., Houser, M., 1984. Phase/doppler spray analyzer for simultaneous measurements of drop size and velocity distributions. Optical Engineering 23 (5), 583–590.

Baer, C., Jaeschke, T., Mertmann, P., Pohl, N., Musch, T., 2014. A MMwave measuring procedure for mass flow monitoring of pneumatic conveyed bulk materials. IEEE Sens. J. 14 (9), 3201–3209.

Balachandar, S., 2024. Fundamentals of Dispersed Multiphase Flows. Cambridge University Press, New York, NY.

Balachandar, S., Eaton, J., 2010. Dispersed turbulent multiphase flow. Annu Rev. Fluid. Mech. 42, 111–133.

Balachandar, S., Zaleski, S., Soldati, A., Ahmadi, G., Bourouiba, L., 2020. Host-to-host airborne transmission as a multiphase flow problem for science-based social distance guidelines. Int. J. Multiph. Flow 132, 103439.

Banko, A.J., Benson, M.J., Gunady, I.E., Elkins, C.J., Eaton, J.K., 2020. An improved three-dimensional concentration measurement technique using magnetic resonance imaging. Exp. Fluids. 61 (2), 53.

Banko, A.J., Coletti, F., Schiavazzi, D., Elkins, C.J., Eaton, J.K., 2015. Three-dimensional inspiratory flow in the upper and central human airways. Exp. Fluids. 56 (6), 1–12.

Basha, N., Arcucci, R., Angeli, P., Anastasiou, C., Abadie, T., Casas, C.Q., Chen, J., Cheng, S., Chagot, L., Galvanin, F., 2024. Machine learning and physics-driven modelling and simulation of multiphase systems. Int. J. Multiph. Flow 179, 104936.

Bateson, C.P., Aliseda, A., 2012. Wind tunnel measurements of the preferential concentration of inertial droplets in homogeneous isotropic turbulence. Exp. Fluids. 52, 1373–1387.

Benson, M.J., Banko, A.J., Elkins, C.J., An, D.-G., Song, S., Bruschewski, M., Grundmann, S., Bandopadhyay, T., Roca, L.V., Sutton, B., Han, K., Hwang, W., Eaton, J.K., 2023. MRV challenge 2: phase locked turbulent measurements in a roughness array. Exp. Fluids. 64 (2), 28.

Benson, M.J., Banko, A.J., Elkins, C.J., An, D.-G., Song, S., Bruschewski, M., Grundmann, S., Borup, D.D., Eaton, J.K., 2020. The 2019 MRV challenge: turbulent flow through a U-bend. Exp. Fluids. 61 (6), 148.

Benson, M.J., Elkins, C.J., Mobley, P.D., Alley, M.T., Eaton, J.K., 2010. Three-dimensional concentration field measurements in a mixing layer using magnetic resonance imaging. Exp. Fluids. 49 (1), 43–55.

Biasiori-Poulanges, L., Bourquard, C., Lukić, B., Broche, L., Supponen, O., 2023. Synchrotron X-ray imaging of the onset of ultrasonic horn cavitation. Ultrason. Sonochem. 92, 106286.

Bieberle, A., Härting, H.-U., Rabha, S., Schubert, M., Hampel, U., 2013. Gamma-ray computed tomography for imaging of multiphase flows. Chemie Ingenieur Technik 85 (7), 1002–1011.

Black, D.L., McQuay, M.Q., 2001. Laser-based particle measurements of spherical and nonspherical particles. Int. J. Multiph. Flow 27 (8), 1333–1362.

Bo, O.L., Nyfors, E., 2002. Application of microwave spectroscopy for the detection of water fraction and water salinity in water/oil/gas pipe flow. J. Non. Cryst. Solids. 305 (1-3), 345–353.

Borup, D.D., Elkins, C.J., Eaton, J.K., 2018. Development and validation of an MRI-based method for 3D particle concentration measurement. Int. J. Heat. Fluid. Flow. 71, 275–287.
Bothell, J.K., Machicoane, N., Li, D., Morgan, T.B., Aliseda, A., Kastengren, A.L., Heindel, T.J., 2020. Comparison of X-ray and optical measurements in the near-field of an optically dense coaxial air-assisted atomizer. Int. J. Multiph. Flow 125, 103219.
Bothell, J.K., Morgan, T.B., Kastengren, A.L., Heindel, T.J., 2022. Fluid flow observations of the spray near-field using high-speed X-ray imaging. Journal of Flow Visualization and Image Processing 29 (2), 1–26.
Bourouiba, L., 2021. The fluid dynamics of disease transmission. Annu Rev. Fluid. Mech. 53 (1), 473–508.
Brandt, L., Coletti, F., 2022. Particle-laden turbulence: progress and perspectives. Annu Rev. Fluid. Mech. 54, 159–189.
Bremhorst, K., Gilmore, D., 1976. Response of hot wire anemometer probes to a stream of air bubbles in a water flow. J. Phys. e 9 (5), 347.
Brendel, L.P., Weibel, J.A., Braun, J.E., Groll, E.A., 2023. Microgravity two-phase flow research in the context of vapor compression cycle experiments on parabolic flights. Int. J. Multiph. Flow 160, 104358.
Brennen, C.E., 2015. Cavitation in medicine. Interface Focus. 5 (5), 20150022.
Brown, R.W., Cheng, Y.C.N., Haacke, E.M., Thompson, M.R., Venkatesan, R., 2014. Magnetic Resonance Imaging: Physical Principles and Sequence Design. John Wiley & Sons.
Bruschewski, M., Freudenhammer, D., Buchenberg, W.B., Schiffer, H.-P., Grundmann, S., 2016. Estimation of the measurement uncertainty in magnetic resonance velocimetry based on statistical models. Exp. Fluids. 57 (5), 83.
Bruschewski, M., Wüstenhagen, C., Domnick, C., Krewinkel, R., Shiau, C.-C., Grundmann, S., Han, J.-C., 2023. Assessment of the flow field and heat transfer in a vane cooling system using magnetic resonance velocimetry, thermochromic liquid crystals, and computational fluid dynamics. J. Turbomach. 145 (3), 031010.
Brutin, D., Sobac, B., Rigollet, F., Le Niliot, C., 2011. Infrared visualization of thermal motion inside a sessile drop deposited onto a heated surface. Exp. Therm. Fluid. Sci. 35 (3), 521–530.
Bruun, H.H., 1995. Hot-Wire Anemometry: Principles and Signal Analysis. Oxford University Press.
Bryan, S., Clarke, A., Vanderkluysen, L., Groppi, C., Paine, S., Bliss, D.W., Aberle, J., Mauskopf, P., 2017. Measuring water vapor and ash in volcanic eruptions with a millimeter-wave radar/imager. IEEE Transactions on Geoscience and Remote Sensing 55 (6), 3177–3185.
Callaghan, P.T., 1993. Principles of Nuclear Magnetic Resonance Microscopy. Clarendon Press.
Capecelatro, J., Wagner, J.L., 2024. Gas–particle dynamics in high-speed flows. Annu Rev. Fluid. Mech. 56, 379–403.
Cartellier, A., 1992a. Local velocity and size measurements of particles in dense suspensions: theory and design of endoscopic grating velocimeter–Granulometers. Appl. Opt. 31 (18), 3493–3505.
Cartellier, A., 1992b. Simultaneous void fraction measurement, bubble velocity, and size estimate using a single optical probe in gas–liquid two-phase flows. Review of Scientific Instruments 63 (11), 5442–5453.
Cartellier, A., Achard, J., 1991. Local phase detection probes in fluid/fluid two-phase flows. Review of Scientific Instruments 62 (2), 279–303.
Ceccio, S.L., George, D.L., 1996. A review of electrical impedance techniques for the measurement of multiphase flows. J. Fluids. Eng. 118, 391–399.
Chaouki, J., Larachi, F., Dudukovic, M.P., 1997. Noninvasive tomography and velocimetric monitoring of multiphase flows. Ind. Eng. Chem. Res. 36, 4476–4503.
Chen, X., Zhong, W., Heindel, T.J., 2019a. Orientation of cylindrical particles in a fluidized bed based on stereo X-ray particle tracking velocimetry (XPTV). Chem. Eng. Sci. 203, 104–112.
Chen, X., Zhong, W., Heindel, T.J., 2019b. Using stereo XPTV to determine cylindrical particle distribution and velocity in a binary fluidized bed. AIChE Journal 65 (2), 520–535.
Cho, J., Perlin, M., Ceccio, S.L., 2005. Measurement of near-wall stratified bubbly flows using electrical impedance. Measurement Science and Technology 16 (4), 1021.
Clark, A., Machicoane, N., Aliseda, A., 2019. A quantitative study of track initialization of the four-frame best estimate algorithm for three-dimensional Lagrangian particle tracking. Measurement Science and Technology 30 (4), 045302.
Clarke, D.A., Hogendoorn, W., Penn, A., Serial, M.R., 2023. Magnetic resonance imaging in granular flows: an overview of recent advances. Particuology.
Corcoran, T.E., Hitron, R., Humphrey, W., Chigier, N., 2000. Optical measurement of nebulizer sprays: A quantitative comparison of diffraction, phase doppler interferometry, and time of flight techniques. J. Aerosol. Sci. 31 (1), 35–50.
Coussios, C.C., Roy, R.A., 2008. Applications of acoustics and cavitation to noninvasive therapy and drug delivery. Annu Rev. Fluid. Mech. 40 (1), 395–420.
Cuesta, C.J., Davies, J., Worrall, K., Cammarano, A., Zare-Behtash, H., 2025. Plume-surface interactions: A review of experimental work. Acta Astronaut. 226, 892–912.
Cui, Z., Wang, Q., Xue, Q., Fan, W., Zhang, L., Cao, Z., Sun, B., Wang, H., Yang, W., 2016. A review on image reconstruction algorithms for electrical capacitance/resistance tomography. Sensor Review 36 (4), 429–445.
Cui, Z., Zhang, Q., Gao, K., Xia, Z., Wang, H., 2021. Electrical impedance sensors for multi-phase flow measurement: A review. IEEE Sens. J. 21 (24), 27252–27267.
Da, Silva, M.J., 2008. PhD Thesis. Technische Universität Dresden, Dresden, Germany.
Da Silva, M.J., Schleicher, E., Hampel, U., 2007. A novel needle probe based on high-speed complex permittivity measurements for investigation of dynamic fluid flows. IEEE Trans. Instrum. Meas. 56 (4), 1249–1256.
Dauxois, T., Peacock, T., Bauer, P., Caulfield, C.P., Cenedese, C., Gorlé, C., Haller, G., Ivey, G.N., Linden, P.F., Meiburg, E., Pinardi, N., Vriend, N.M., Woods, A.W., 2021. Confronting grand challenges in environmental fluid mechanics. Phys. Rev. Fluids. 6 (2), 020501.
de Mesquita, C.H., Velo, A.F., Carvalho, D.V.S., Martins, J.F.T., Hamada, M.M., 2016. Industrial tomography using three different gamma ray. Flow Measurement and Instrumentation 47, 1–9.
Deike, L., 2022. Mass transfer at the ocean–atmosphere interface: the role of wave breaking, droplets, and bubbles. Annu Rev. Fluid. Mech. 54 (1), 191–224.
Deike, L., Ghabache, E., Liger-Belair, G., Das, A.K., Zaleski, S., Popinet, S., Séon, T., 2018. Dynamics of jets produced by bursting bubbles. Phys. Rev. Fluids. 3 (1), 013603.
Delhaye, J., 1969. Hot-film anemometry in two-phase flow. In: ASME Symposium on Two-phase Flow Instrumentation, 11th National Heat Transfer Conference, pp. 58–69.
Delnoij, E., Westerweel, J., Deen, N.G., Kuipers, J., Van Swaaij, W., 1999. Ensemble correlation PIV applied to bubble plumes rising in a bubble column. Chem. Eng. Sci. 54 (21), 5159–5171.
Di Marco, P., Kim, J., Ohta, H., Cheng, L., Mewes, D., 2009. Boiling heat transfer in reduced gravity environments. Advances in Multiphase Flow and Heat Transfer 1, 53–92.
Di Renzo, M., Urzay, J., 2018. Aerodynamic generation of electric fields in turbulence laden with charged inertial particles. Nat. Commun. 9 (1), 1676.
Dumoulin, C.L., Souza, S.P., Walker, M.F., Wagle, W., 1989. Three-dimensional phase contrast angiography. Magn. Reson. Med. 9 (1), 139–149.
Dworzanczyk, A., Viqueira-Moreira, M., Langhorn, J., Libeau, M., Brehm, C., Parziale, N., 2025. On aerobreakup in the stagnation region of high-mach-number flow over a bluff body. J. Fluid. Mech. 1002, A1.
Efhaima, A., Al-Dahhan, M.H., 2015. Local time-averaged gas holdup in fluidized bed reactor using gamma ray computed tomography technique (CT). International Journal of Industrial Chemistry 6 (3), 143–152.
Elbing, B.R., Winkel, E.S., Lay, K.A., Ceccio, S.L., Dowling, D.R., Perlin, M., 2008. Bubble-induced skin-friction drag reduction and the abrupt transition to air-layer drag reduction. J. Fluid. Mech. 612, 201–236.
Elghobashi, S., 2019. Direct numerical simulation of turbulent flows laden with droplets or bubbles. Annu Rev. Fluid. Mech. 51 (1), 217–244.
Elkins, C.J., Alley, M.T., 2007. Magnetic resonance velocimetry: applications of magnetic resonance imaging in the measurement of fluid motion. Exp. Fluids. 43 (6), 823–858.
Elkins, C.J., Alley, M.T., Saetran, L., Eaton, J.K., 2009. Three-dimensional magnetic resonance velocimetry measurements of turbulence quantities in complex flow. Exp. Fluids. 46, 285–296.
Elkins, C.J., Markl, M., Pelc, N., Eaton, J.K., 2003. 4D magnetic resonance velocimetry for mean velocity measurements in complex turbulent flows. Exp. Fluids. 34 (4), 494–503.
Ergin, F.G., 2017. Dynamic masking techniques for particle image velocimetry. Isı Bilimi ve Tekniği Dergisi 37 (2), 61–74.
Esmaily, M., Villafane, L., Banko, A., Iaccarino, G., Eaton, J., Mani, A., 2020. A benchmark for particle-laden turbulent duct flow: A joint computational and experimental study. Int. J. Multiph. Flow 132, 103410.
Fan, J., Wang, F., 2021. Review of ultrasonic measurement methods for two-phase flow. Rev. Sci. Instruments 92 (9), 091502.
Farrar, B., Bruun, H., 1989. Interaction effects between a cylindrical hot-film anemometer probe and bubbles in air/water and oil/water flows. J. Phys. e 22 (2), 114.
Farrar, B., Samways, A., Ali, J., Bruun, H., 1995. A computer-based hot-film technique for two-phase flow measurements. Measurement Sci. Technol. 6 (10), 1528–1537.
Fdida, N., Blaisot, J.-B., 2009. Drop size distribution measured by imaging: determination of the measurement volume by the calibration of the point spread function. Meas. Sci. Technol. 21 (2), 025501.
Felton, K., Loth, E., 2002. Diffusion of spherical bubbles in a turbulent boundary layer. Int. J. Multiph. Flow 28 (1), 69–92.
Ferran, A., Machicoane, N., Aliseda, A., Obligado, M., 2023. An experimental study on the settling velocity of inertial particles in different homogeneous isotropic turbulent flows. J. Fluid. Mech. 970, A23.
Fessler, J.A., 2020. Optimization methods for magnetic resonance image reconstruction: key models and Optimization algorithms. IEEE Signal. Process. Mag. 37 (1), 33–40.
Figueiredo, M.M.F., Goncalves, J.L., Nakashima, A.M.V., Fileti, A.M.F., Carvalho, R.D.M., 2016. The use of an ultrasonic technique and neural networks for identification of the flow pattern and measurement of the gas volume fraction in multiphase flows. Exp. Therm. Fluid. Sci. 70, 29–50.
Foster, C.W., Oruganti, S., Panerai, F., 2025. Super-resolved microstructure of pyrolyzing superlight ablators. Npj. Mater. Degrad. 9 (1), 9.
Fox, R.O., 2012. Large-eddy-simulation tools for multiphase flows. Annu Rev. Fluid. Mech. 44 (1), 47–76.
Fu, M., Zhao, B., Carignan, C., Shosted, R.K., Perry, J.L., Kuehn, D.P., Liang, Z.-P., Sutton, B.P., 2015. High-resolution dynamic speech imaging with joint low-rank and sparsity constraints. Magn. Reson. Med. 73 (5), 1820–1832.
Fukushima, E., 1999. Nuclear magnetic resonance as a tool to study flow. Annu Rev. Fluid. Mech. 31, 95–123.
Fuster, D., Matas, J.-P., Marty, S., Popinet, S., Hoepffner, J., Cartellier, A., Zaleski, S., 2013. Instability regimes in the primary breakup region of planar coflowing sheets. J. Fluid. Mech. 736, 150–176.
Ganesh, H., Mäkiharju, S.A., Ceccio, S.L., 2016. Bubbly shock propagation as a mechanism for sheet-to-cloud transition of partial cavities. J. Fluid. Mech. 802, 37–78.
Gao, J., Katz, J., 2018. Self-calibrated microscopic dual-view tomographic holography for 3D flow measurements. Opt. Express. 26 (13), 16708–16725.
Garivalis, A.I., Di Marco, P., 2022. Isolated bubbles growing and detaching within an electric field in microgravity. Appl. Therm. Eng. 212, 118538.

Gennarelli, G., Romeo, S., Scarfì, M.R., Soldovieri, F., 2013. A microwave resonant sensor for concentration measurements of liquid solutions. IEEE Sens. J. 13 (5), 1857–1864.
George, D.L., Iyer, C.O., Ceccio, S.L., 2000a. Measurement of the bubbly flow beneath partial attached cavities using electrical impedance probes. J. Fluids. Eng. 122 (1), 151–155.
George, D.L., Shollenberger, K.A., Torczynski, J.R., O'Hern, T.J., Ceccio, S.L., 2001. Three-phase material distribution measurements in a vertical flow using gamma-densitometry tomography and electrical-impedance tomography. Int. J. Multiph. Flow 27 (11), 1903–1930.
George, D.L., Torczynski, J.R., Shollenberger, K.A., O'Hern, T.J., Ceccio, S.L., 2000b. Validation of electrical-impedance tomography for measurements of material distribution in two-phase flows. Int. J. Multiph. Flow 26, 549–581.
Gladden, L.F., Sederman, A.J., 2017. Magnetic resonance imaging and velocity mapping in chemical engineering applications. Annu Rev. Chem. Biomol. Eng. 8 (1), 227–247.
Glovnea, R., Forrest, A., Olver, A., Spikes, H., 2003. Measurement of sub-nanometer lubricant films using ultra-thin film interferometry. Tribol. Lett. 15, 217–230.
Grundmann, S., Wassermann, F., Lorenz, R., Jung, B., Tropea, C., 2012. Experimental investigation of helical structures in swirling flows. Int. J. Heat. Fluid. Flow. 37, 51–63.
Guet, S., Fortunati, R.V., Mudde, R.F., Ooms, G., 2003. Bubble velocity and size measurement with a four-point optical fiber probe. Particle & Particle Systems Characterization: Measurement and Description of Particle Properties and Behavior in Powders and Other Disperse Systems 20 (3), 219–230.
Hampel, U., 2023, "Multiphase imaging techniques," in: *Handbook of Multiphase Flow Science and Technology*, Yeoh, G.H., Joshi, J.B. (Eds.), Springer, Singapore, pp. 591-624.
Hao, X.-Y., Li, X.-B., Zhang, H.-N., Zhang, W.-H., Li, F.-C., 2023. Review on multi-parameter simultaneous measurement techniques for multiphase flow-part B: basic physical parameters and phase characteristics. Measurement 220, 113397.
Hartfuss, H., Geist, T., Hirsch, M., 1997. Heterodyne methods in millimetre wave plasma diagnostics with applications to ECE, interferometry and reflectometry. Plasma Phys. Control Fusion. 39 (11), 1693.
Hassan, Y., Blanchat, T., Seeley Jr, C., Canaan, R., 1992. Simultaneous velocity measurements of both components of a two-phase flow using particle image velocimetry. Int. J. Multiph. Flow 18 (3), 371–395.
Heath, R.W., Gonzalez-Prelcic, N., Rangan, S., Roh, W., Sayeed, A.M., 2016. An overview of signal processing techniques for millimeter wave MIMO systems. IEEE J. Sel. Top. Signal Process. 10 (3), 436–453.
Heindel, T.J., 2011. A review of X-ray flow visualization with applications to multiphase flows. J. Fluids. Eng. 133 (7), 074001.
Heindel, T.J., 2018. X-ray imaging techniques to quantify spray characteristics in the near-field. Atomization and Sprays 28 (11), 1029–1059.
Heindel, T.J., 2024. X-ray flow visualization: techniques and applications. J. Fluids. Eng. 146 (1), 010801.
Hernandez-Alvarado, F., Kalaga, D.V., Turney, D., Banerjee, S., Joshi, J.B., Kawaji, M., 2017. Void fraction, bubble size and interfacial area measurements in co-current downflow bubble column reactor with microbubble dispersion. Chem. Eng. Sci. 168, 403–413.
Hessenkemper, H., Starke, S., Atassi, Y., Ziegenhein, T., Lucas, D., 2022. Bubble identification from images with machine learning methods. Int. J. Multiph. Flow 155, 104169.
Hewitt, G.F., 1978. Measurement of Two Phase Flow Parameters. Academic Press, New York.
Hishida, K., Ando, A., Maeda, M., 1992. Experiments on particle dispersion in a turbulent mixing layer. Int. J. Multiph. Flow 18 (2), 181–194.
Hoffman, D.W., Villafañe, L., Elkins, C.J., Eaton, J.K., 2020. Experimental study of flow inside a centrifugal fan using magnetic resonance velocimetry. J. Eng. Gas. Turbine Power. 142 (4), 041019.
Hoffmann, R., Kögl, T., 2017. An ATEX-proof gamma tomography setup for measuring liquid distribution in process equipment. Flow Measurement and Instrumentation 53, 147–153.
Hogan, R.J., Illingworth, A.J., Sauvageot, H., 2000. Measuring crystal size in cirrus using 35-and 94-GHz radars. J. Atmos. Ocean. Technol. 17 (1), 27–37.
Honkanen, M., Nobach, H., 2005. Background extraction from double-frame PIV images. Exp. Fluids. 38 (3), 348–362.
Hort, M., Scharff, L., 2016. Detection of airborne volcanic ash using radar. Volcanic Ash. Elsevier, pp. 131–160.
Hossein, F., Materazzi, M., Lettieri, P., Angeli, P., 2021. Application of acoustic techniques to fluid-particle systems – A review. Chemical Engineering Research and Design 176, 180–193.
Huck, P., Machicoane, N., Volk, R., 2017. A cost-efficient shadow particle tracking velocimetry setup suitable for tracking small objects in a large volume. Procedia IUTAM. 20, 175–182.
Huck, P., Osuna-Orozco, R., Machicoane, N., Aliseda, A., 2022. Spray dispersion regimes following atomization in a turbulent co-axial gas jet. J. Fluid. Mech. 932, A36.
Jin, H., Yang, S., Guo, Z., He, G., Tong, Z., 2005. The axial distribution of holdups in an industrial-scale bubble column with evaluated pressure using γ-ray attenuation approach. Chemical Engineering Journal 115 (1-2), 45.
Johansen, G.A., 2015, "Gamma-ray tomography," in: *Industrial Tomography: Systems and Applications*, Wang, M. (Ed.), Elsevier, Waltham, MA, pp. 197-222.
John, K., Jahangir, S., Gawandalkar, U., Hogendoorn, W., Poelma, C., Grundmann, S., Bruschewski, M., 2020. Magnetic resonance velocimetry in high-speed turbulent flows: sources of measurement errors and a new approach for higher accuracy. Exp. Fluids. 61 (2), 27.
Kaczmarek, M., Osuna-Orozco, R., Huck, P.D., Aliseda, A., Machicoane, N., 2022. Spatial characterization of the flapping instability of a laminar liquid jet fragmented by a swirled gas co-flow. Int. J. Multiph. Flow 152, 104056.
Kastengren, A.L., Ilavsky, J., Fezzaa, K., 2023. The advanced photon source upgrade and its impact on synchrotron spray research. In: ILASS-AMERICAS 2023, 33nd Annual Conference on Liquid Atomization and Spray Systems. Albuquerque, NM, p. 6. May 14-17, 2023.
Kastengren, A.L., Powell, C.F., 2014. Synchrotron X-ray techniques for fluid dynamics. Exp. Fluids. 55 (3), 1–15.
Katz, J., Sheng, J., 2010. Applications of holography in fluid mechanics and particle dynamics. Annu Rev. Fluid. Mech. 42, 531–555.
Kemmerer, B.W., Langton, A.G., Mantovani, J.G., Atkins, A.R., Batcheldor, D.P., Bastin, G.L., 2023. Development of the dust ejecta radar technology (DERT) to determine plume-surface interaction ejecta velocities on planetary surfaces. In: 2023 IEEE International Radar Conference (RADAR), pp. 1–6. Nov 6-10. 2023.
Kemper, P., Küstermann, E., Dreher, W., Helmers, T., Mießner, U., Besser, B., Thöming, J., 2021. Magnetic resonance imaging for non-invasive study of hydrodynamics inside gas-liquid taylor flows. Chem. Eng. Technol. 44 (3), 465–476.
Khalitov, D., Longmire, E.K., 2002. Simultaneous two-phase PIV by two-parameter phase discrimination. Exp. Fluids. 32 (2), 252–268.
Khlifa, I., Vabre, A., Hočevar, M., Fezzaa, K., Fuzier, S., Roussette, O., Coutier-Delgosha, O., 2017. Fast X-ray imaging of cavitating flows. Exp. Fluids. 58 (11), 157.
Khopkar, A.R., Rammohan, A.R., Ranade, V.V., Dudukovic, M.P., 2005. Gas-liquid flow generated by a Rushton turbine in stirred vessel: CARPT/CT measurements and CFD simulations. Chem. Eng. Sci. 60 (8–9), 2215–2229.
Kiger, K., Pan, C., 2000. PIV technique for the simultaneous measurement of dilute two-phase flows. Journal Fluids Engineering 122 (4), 811–818.
Kim, H., Buongiorno, J., 2011. Detection of liquid–vapor–solid triple contact line in two-phase heat transfer phenomena using high-speed infrared thermometry. Int. J. Multiph. Flow 37 (2), 166–172.
Kingston, T.A., Geick, T.A., Robinson, T.R., Heindel, T.J., 2015. Characterizing 3D granular flow structures in a double screw mixer using X-ray particle tracking velocimetry. Powder. Technol. 278, 211–222.
Kleinstreuer, C., Zhang, Z., 2010. Airflow and particle transport in the human respiratory system. Annu Rev. Fluid. Mech. 42 (1), 301–334.
Knop, I., Bansmer, S.E., Hahn, V., Voigt, C., 2021. Comparison of different droplet measurement techniques in the Braunschweig icing wind tunnel. Atmos. Meas. Tech. 14 (2), 1761–1781.
Knowles, P.L., Kiger, K.T., 2012. Quantification of dispersed phase concentration using light sheet imaging methods. Exp. Fluids. 52 (3), 697–708.
Koffman, L.D., Plesset, M.S., 1983. Experimental observations of the microlayer in vapor bubble growth on a heated solid. J. Heat. Transfer. 105 (3), 625–632.
Kollias, P., Albrecht, B., Lhermitte, R., Savtchenko, A., 2001. Radar observations of updrafts, downdrafts, and turbulence in fair-weather cumuli. J. Atmos. Sci. 58 (13), 1750–1766.
Kollias, P., Clothiaux, E.E., Ackerman, T.P., Albrecht, B.A., Widener, K.B., Moran, K.P., Luke, E.P., Johnson, K.L., Bharadwaj, N., Mead, J.B., 2016. Development and applications of ARM millimeter-wavelength cloud radars. Meteorol. Monogr. 57, 17.11–17.19.
Kollias, P., Clothiaux, E.E., Miller, M.A., Albrecht, B.A., Stephens, G.L., Ackerman, T.P., 2007. Millimeter-wavelength radars: new frontier in atmospheric cloud and precipitation research. Bull. Am. Meteorol. Soc. 88 (10), 1608–1624.
Konishi, C., Mudawar, I., 2015. Review of flow boiling and critical heat flux in microgravity. Int. J. Heat. Mass Transf. 80, 469–493.
Kosiwczuk, W., Cessou, A., Trinite, M., Lecordier, B., 2005. Simultaneous velocity field measurements in two-phase flows for turbulent mixing of sprays by means of two-phase PIV. Exp. Fluids. 39 (5), 895–908.
Kossolapov, A., Phillips, B., Bucci, M., 2021. Can LED lights replace lasers for detailed investigations of boiling phenomena? Int. J. Multiph. Flow 135, 103522.
Kulick, J.D., Fessler, J.R., Eaton, J.K., 1994. Particle response and turbulence modification in fully developed channel flow. J. Fluid. Mech. 277, 109–134.
Lasheras, J., Villermaux, E., Hopfinger, E., 1998. Break-up and atomization of a round water jet by a high-speed annular air jet. J. Fluid. Mech. 357, 351–379.
Lauterbur, P.C., 1973. Image formation by induced local interactions: examples employing nuclear magnetic resonance. Nature 242 (5394), 190–191.
Lefebvre, A., Mezui, Y., Obligado, M., Gluck, S., Cartellier, A., 2022. A new, optimized doppler optical probe for phase detection, bubble velocity and size measurements: investigation of a bubble column operated in the heterogeneous regime. Chem. Eng. Sci. 250, 117359.
Leung, W., Revankar, S., Ishii, Y., Ishii, M., 1995. Axial development of interfacial area and void concentration profiles measured by double-sensor probe method. Int. J. Heat. Mass Transf. 38 (3), 445–453.
Li, D., Bothell, J.K., Morgan, T.B., Heindel, T.J., Aliseda, A., Machicoane, N., Kastengren, A.L., 2017. High-speed X-ray imaging of an airblast atomizer at the nozzle exit. In: *2017 APS-DFD Meeting*, Denver, CO, November 19 - 21, 2017, 2017 APS-DFD Gallery of Fluid Motion Video Entry #V0026. https://doi.org/10.1103/APS.DFD.2017.GFM.V0026.
Li, M., Wang, R., Li, W., Chen, H., Min, R., Gao, Z., 2025. Characterization and visualization of gas–liquid two-phase flow based on wire-mesh sensor. Measurement 243, 116265.
Li, X.-B., Hao, X.-Y., Zhang, H.-N., Zhang, W.-H., Li, F.-C., 2023. Review on multi-parameter simultaneous measurement techniques for multiphase flow–Part A: velocity and temperature/pressure. Measurement 223, 113710.
Li, Y., Blois, G., Kazemifar, F., Christensen, K.T., 2021. A particle-based image segmentation method for phase separation and interface detection in PIV images of immiscible multiphase flow. Measurement Sci. Technol. 32 (9), 095208.

Machicoane, N., Bonaventure, J., Volk, R., 2013. Melting dynamics of large ice balls in a turbulent swirling flow. Phys. Fluids 25 (12).

Machicoane, N., Bothell, J.K., Li, D., Morgan, T.B., Heindel, T.J., Kastengren, A.L., Aliseda, A., 2019. Synchrotron radiography characterization of the liquid core dynamics in a canonical two-fluid coaxial atomizer. Int. J. Multiph. Flow 115, 1–8.

Machicoane, N., Ricard, G., Osuna-Orozco, R., Huck, P.D., Aliseda, A., 2020. Influence of steady and oscillating swirl on the near-field spray characteristics in a two-fluid coaxial atomizer. Int. J. Multiph. Flow 129, 103318.

Machicoane, N., Zimmermann, R., Fiabane, L., Bourgoin, M., Pinton, J.-F., Volk, R., 2014. Large sphere motion in a nonhomogeneous turbulent flow. New. J. Phys. 16 (1), 013053.

Mallach, M., Gebhardt, P., Musch, T., 2017. 2D microwave tomography system for imaging of multiphase flows in metal pipes. Flow Measurement Instrument. 53 (A), 80–88.

Mansfield, P., 1977. Multi-planar image formation using NMR spin echoes. J. Phys. C: Solid State Physics 10 (3), L55.

Mantle, M.D., Sederman, A.J., 2003. Dynamic MRI in chemical process and reaction engineering. Prog. Nucl. Magn. Reson. Spectrosc. 43 (1-2), 3–60.

Markl, M., Chan, F.P., Alley, M.T., Wedding, K.L., Draney, M.T., Elkins, C.J., Parker, D. W., Wicker, R., Taylor, C.A., Herfkens, R.J., Pelc, N.J., 2003. Time-resolved three-dimensional phase-contrast MRI. Journal of Magnetic Resonance Imaging 17 (4), 499–506.

Markl, M., Frydrychowicz, A., Kozerke, S., Hope, M., Wieben, O., 2012. 4D flow MRI. J. Magnet. Resonance Imag. 36 (5), 1015–1036.

Martin, J.E., García, M.H., 2009. Combined PIV/PLIF measurements of a steady density current front. Exp. Fluids. 46 (2), 265–276.

Masuk, A.U.M., Salibindla, A., Ni, R., 2019. A robust virtual-camera 3D shape reconstruction of deforming bubbles/droplets with additional physical constraints. Int. J. Multiphase Flow 120, 103088.

Maurice, G., Machicoane, N., Barre, S., Djeridi, H., 2021. Coupled X-ray high-speed imaging and pressure measurements in a cavitating backward facing step flow. Phys. Rev. Fluids. 6 (4), 044311.

Mééès, L., Grosjean, N., Marié, J.L., Fournier, C., 2020. Statistical Lagrangian evaporation rate of droplets released in a homogeneous quasi-isotropic turbulence. Phys. Rev. Fluids. 5 (11), 113602.

Meola, C., Carlomagno, G.M., 2004. Recent advances in the use of infrared thermography. Measurement Sci. Technol. 15 (9), R27.

Monrós-Andreu, G., Martinez-Cuenca, R., Torró, S., Escrig, J., Hewakandamby, B., Chiva, S., 2016. Multi-needle capacitance probe for non-conductive two-phase flows. Measurement Sci. Technol. 27 (7), 074004.

Mora, D.O., Obligado, M., Aliseda, A., Cartellier, A., 2021. Effect of Re_λ and Rouse numbers on the settling of inertial droplets in homogeneous isotropic turbulence. Phys. Rev. Fluids. 6 (4), 044305.

Morimoto, M., Fukami, K., Fukagata, K., 2021. Experimental velocity data estimation for imperfect particle images using machine learning. Phys. Fluids 33 (8).

Munholand, L., Soucy, G., 2005. Comparison of four conductive needle probe designs for determination of bubble velocity and local gas holdup. Rev. Sci. Instrument. 76 (9).

Nadeem, H., Jamdagni, P., Subramaniam, S., Nere, N.K., Heindel, T.J., 2023. Assessing solid particle mixing using X-ray radiographic particle tracking. Chem. Eng. Res. Des. 194, 563–572.

Nejati, I., Sielaff, A., Franz, B., Zimmermann, M., Hänichen, P., Schweikert, K., Krempel, J., Stephan, P., Martin, A., Scheerer, H., 2020. Experimental investigation of single bubble nucleate boiling in microgravity. Microgravity. Sci. Technol. 32, 597–607.

Ni, R., 2024. Deformation and breakup of bubbles and drops in turbulence. Annu Rev. Fluid. Mech. 56, 319–347.

Nishio, S., Gotoh, T., Nagai, N., 1998. Observation of boiling structures in high heat-flux boiling. Int. J. Heat. Mass Transf. 41 (21), 3191–3201.

Nyfors, E., 2000. Industrial microwave sensors - a review. Subsurface Sens. Technol. Applic. 1 (1), 23–43.

Oakley, T., Loth, E., Adrian, R., 1997. A two-phase cinematic PIV method for bubbly flows. J. Fluids Eng. 119 (3), 707–712.

Oue, M., Kumjian, M.R., Lu, Y., Jiang, Z., Clothiaux, E.E., Verlinde, J., Aydin, K., 2015. X-band polarimetric and Ka-band doppler spectral radar observations of a graupel-producing arctic mixed-phase cloud. J. Appl. Meteorol. Climatol. 54 (6), 1335–1351.

Ouellette, N.T., Xu, H., Bodenschatz, E., 2006. A quantitative study of three-dimensional Lagrangian particle tracking algorithms. Exp. Fluids. 40, 301–313.

Pal, R., 1994. Techniques for measuring the composition (oil and water content) of emulsions—A state of the art review. Colloids Surf. A: Physicochem. Eng. Aspects 84 (2–3), 141–193.

Parker, J.T., Dreier, T., Nilsson, D., Mäkiharju, S.A., 2024. In-lab X-ray particle velocimetry for multiphase flows: design principles and demonstration of O(1 kHz) XPV. Flow Measurement Instrument. 96, 102536.

Pelc, N.J., Bernstein, M.A., Shimakawa, A., Glover, G.H., 1991a. Encoding strategies for three-direction phase-contrast MR imaging of flow. J. Magnet. Resonance Imag. 1 (4), 405–413.

Pelc, N.J., Herfkens, R.J., Shimakawa, A., Enzmann, D.R., 1991b. Phase contrast cine magnetic resonance imaging. Magn. Reson. Q. 7 (4), 229–254.

Peña, H.V., Rodriguez, O., 2015. Applications of wire-mesh sensors in multiphase flows. Flow Measurement Instrument. 45, 255–273.

Pillers, R.A., Heindel, T.J., 2023. Plume analysis of plunging liquid jets with floor interactions using stereographic backlit imaging. J. Flow Visualiz. Image Process. 30 (4), 1–23.

Poelma, C., 2016. Ultrasound imaging velocimetry: A review. Exp. Fluids. 58 (1), 3.

Poelma, C., 2020. Measurement in opaque flows: A review of measurement techniques for dispersed multiphase flows. Acta Mech. 231 (6), 2089–2111.

Poelma, C., Westerweel, J., Ooms, G., 2006. Turbulence statistics from optical whole-field measurements in particle-laden turbulence. Exp. Fluids. 40 (3), 347–363.

Polese, M., Cantos-Roman, X., Singh, A., Marcus, M.J., Maccarone, T.J., Melodia, T., Jornet, J.M., 2023. Coexistence and spectrum sharing above 100 GHz. In: Proceedings of the IEEE, 111, pp. 928–954.

Powell, R.L., 2008. Experimental techniques for multiphase flows. Phys. Fluids 20 (4), 040605–040622.

Prasser, H.-M., Scholz, D., Zippe, C., 2001. Bubble size measurement using wire-mesh sensors. Flow Measurement and Instrument. 12 (4), 299–312.

Qiu, H.-H., Sommerfeld, M., 1992. A reliable method for determining the measurement volume size and particle mass fluxes using phase-doppler anemometry. Exp. Fluids. 13 (6), 393–404.

Qiu, H., Jia, W., Hsu, C.-T., 2001. Optimization of optical particle sizing in multiphase flows. Opt. Eng. 40 (11), 2586–2593.

Quintino, A.M., da Rocha, D.L.L.N., Fonseca Júnior, R., Rodriguez, O.M.H., 2021. Flow pattern transition in pipes using data-driven and physics-informed machine learning. J. Fluids. Eng. 143 (3), 031401.

Rácz, E., Malý, M., Jedelský, J., Józsa, V., 2022. Gas-phase velocity estimation in practical sprays by phase-doppler technique. Int. J. Multiph. Flow 157, 104260.

Rahimi, A., Ejtehadi, O., Lee, K., Myong, R., 2020. Near-field plume-surface interaction and regolith erosion and dispersal during the lunar landing. Acta Astronaut. 175, 308–326.

Rasel, R.K., Chowdhury, S.M., Marashdeh, Q.M., Teixeira, F.L., 2022. Review of selected advances in electrical capacitance volume tomography for multiphase flow monitoring. Energies. (Basel) 15 (14), 5285.

Rasmont, N., Al-Rashdan, H., Elliott, G., Rovey, J.L., Villafañe, L., 2024. Millimeter-wave tomographic interferometry of ejecta concentrations in plume-surface interactions. AIAA SCITECH 2024 Forum. AIAA 2024-1979.

Rasmont, N., Al-Rashdan, H.T., Elliott, G., Rovey, J.L., Villafañe, L., 2023. Millimeter-wave interferometry for opaque particle-laden flows. IEEE Trans. Microw. Theory. Tech. 71 (11), 4893–4905.

Rasmont, N., Heuser, L., Rovey, J., Villafañe Roca, L., 2025a, "Multiple approach for ejecta mapping in PSI: millimeter-wave tomography coupled with PTV and predictive modeling," *AIAA SCITECH 2025 Forum*, January 6-10, 2025, Orlando, FL p. 2400.

Rasmont, N., Rovey, J., Villafane, L., 2025b. "Validation and Calibration of a Millimeter Wave Interferometer for Concentration Measurements in Particle-Laden Flows". Int. J. Multiph. Flow. Accepted for publication, *Available at SSRN 5022662*.

Ricard, G., Machicoane, N., Osuna-Orozco, R., Huck, P.D., Aliseda, A., 2021. Role of convective acceleration in the interfacial instability of liquid-gas coaxial jets. Phys. Rev. Fluids. 6 (8), 084302.

Rieke, V., Butts Pauly, K., 2008. MR thermometry. J. Magnet. Resonance Imag. 27 (2), 376–390.

Rogers, C., Eaton, J., 1991. The effect of small particles on fluid turbulence in a flat-plate, turbulent boundary layer in air. Phys. Fluids A Fluid Dyn. 3 (5), 928–937.

Roisman, I.V., Tropea, C., 2001. Flux measurements in sprays using phase doppler techniques. Atomization and Sprays 11 (6), 667–699.

Rottenkolber, G., Gindele, J., Raposo, J., Dullenkopf, K., Hentschel, W., Wittig, S., Spicher, U., Merzkirch, W., 2002. Spray analysis of a gasoline direct injector by means of two-phase PIV. Exp. Fluids. 32, 710–721.

Sankar, S., Weber, B., Kamemoto, D., Bachalo, W., 1991. Sizing fine particles with the phase doppler interferometric technique. Appl. Opt. 30 (33), 4914–4920.

Seifi, M., Fournier, C., Grosjean, N., Mééès, L., Marié, J.-L., Denis, L., 2013. Accurate 3D tracking and size measurement of evaporating droplets using in-line digital holography and "inverse problems" reconstruction approach. Opt. Express. 21 (23), 27964–27980.

Seol, D.-G., Bhaumik, T., Bergmann, C., Socolofsky, S.A., 2007. Particle image velocimetry measurements of the mean flow characteristics in a bubble plume. J. Eng. Mech. 133 (6), 665–676.

Serial, M.R., Benders, S., Rotzetter, P., Brummerloh, D.L., Metzger, J.P., Gross, S.P., Nussbaum, J., Müller, C.R., Pruessmann, K.P., Penn, A., 2023. Temperature distribution in a gas-solid fixed bed probed by rapid magnetic resonance imaging. Chem. Eng. Sci. 269, 118457.

Shaikh, A., Taha, M.M., Al-Dahhan, M.H., 2021. Phase distribution in Fischer-Tropsch mimicked slurry bubble column via computed tomography. Chem. Eng. Sci. 231, 116278.

Shaikh, A., Taha, M.M., Al-Dahhan, M.H., 2023. Phases distribution in slurry bubble columns: insights from single-source computed tomography and gas holdup measurements. Flow Measurem. Instrument. 93, 102441.

Sielaff, A., Gowik, M., Völzel, C., Rosengarten, G., Rajic, N., Stephan, P., 2019. Temperature measurement using infrared thermometry within semi-transparent Media. Exp. Heat Transf. 32 (6), 545–565.

Sielaff, A., Mangini, D., Kabov, O., Raza, M.Q., Garivalis, A.I., Zupančič, M., Dehaeck, S., Evgenidis, S., Jacobs, C., Van Hoof, D., 2022. The multiscale boiling investigation on-board the International Space Station: an overview. Appl. Therm. Eng. 205, 117932.

Sleiman, H.C., Tengattini, A., Briffaut, M., Huet, B., Dal Pont, S., 2021. Simultaneous X-ray and neutron 4D tomographic study of drying-driven hydro-mechanical behavior of cement-based materials at moderate temperatures. Cem. Concr. Res. 147, 106503.

Snoek, C.W., 1990. A selection of new developments in multiphase flow measurement techniques. Exp. Therm. Fluid. Sci. 3, 60–73.

Soltanaghaei, E., Prabhakara, A., Balanuta, A., Anderson, M., Rabaey, J.M., Kumar, S., Rowe, A., 2021. Millimetro: MMwave retro-reflective tags for accurate, long range localization. In: Proceedings of the 27th Annual International Conference on Mobile Computing and Networking, pp. 69–82.

Soulez, F., Denis, L., Thiébaut, É., Fournier, C., Goepfert, C., 2007. Inverse problem approach in particle digital holography: out-of-field particle detection made possible. J. Opt. Soc. Am. A 24 (12), 3708–3716.
Stamati, O., Marks, B., Andò, E., Roux, S., Machicoane, N., 2023. X-ray radiography 4D particle tracking of heavy spheres suspended in a turbulent jet. Int. J. Multiphase Flow 162, 104406.
Stannarius, R., 2017. Magnetic resonance imaging of granular materials. Rev. Sci. Instrum. 88 (5).
Stride, E., Coussios, C., 2019. Nucleation, mapping and control of cavitation for drug delivery. Nat. Rev. Phys. 1 (8), 495–509.
Subramaniam, S., 2020. Multiphase flows: rich physics, challenging theory, and big simulations. Phys. Rev. Fluids. 5 (11), 110520.
Subramaniam, S., Balachandar, S., 2022. Modeling Approaches and Computational Methods for Particle-Laden Turbulent Flows. Elsevier.
Sultan, A.J., Sabri, L.S., Al-Dahhan, M.H., 2018. Impact of heat-exchanging tube configurations on the gas holdup distribution in bubble columns using gamma-ray computed tomography. Int. J. Multiphase Flow 106, 202–219.
Sun, S., Rappaport, T.S., Heath, R.W., Nix, A., Rangan, S., 2014. MIMO for millimeter-wave wireless communications: beamforming, spatial multiplexing, or both? IEEE Commun. Magazine 52 (12), 110–121.
Surtaev, A., Serdyukov, V., Zhou, J., Pavlenko, A., Tumanov, V., 2018. An experimental study of vapor bubbles dynamics at water and ethanol pool boiling at low and high heat fluxes. Int. J. Heat. Mass Transf. 126, 297–311.
Tan, C., Murai, Y., Liu, W., Tasaka, Y., Dong, F., Takeda, Y., 2021. Ultrasonic doppler technique for application to multiphase flows: A review. Int. J. Multiphase Flow 144, 103811.
Tan, S., Salibindla, A., Masuk, A.U.M., Ni, R., 2020. Introducing OpenLPT: new method of removing ghost particles and high-concentration particle shadow tracking. Exp. Fluids. 61, 1–16.
Tanaka, T., Eaton, J.K., 2010. Sub-Kolmogorov resolution particle image velocimetry measurements of particle-laden forced turbulence. J. Fluid. Mech. 643, 177–206.
Tapp, H.S., Peyton, A., Kemsley, E.K., Wilson, R.H., 2003. Chemical engineering applications of electrical process tomography. Sens. Actuat. B: Chem. 92 (1-2), 17–24.
Tayler, A.B., Holland, D.J., Sederman, A.J., Gladden, L.F., 2012a. Applications of ultra-fast MRI to high voidage bubbly flow: measurement of bubble size distributions, interfacial area and hydrodynamics. Chem. Eng. Sci. 71, 468–483.
Tayler, A.B., Holland, D.J., Sederman, A.J., Gladden, L.F., 2012b. Exploring the origins of turbulence in multiphase flow using compressed sensing MRI. Phys. Rev. Lett. 108 (26), 264505.
Tecchio, C., Zhang, X., Cariteau, B., Zalczer, G., Roca i Cabarrocas, P., Bulkin, P., Charliac, J., Vassant, S., Nikolayev, V.S., 2024. Microlayer in nucleate boiling seen as Landau–Levich film with dewetting and evaporation. J. Fluid. Mech. 989 (A4).
Theofanous, T., Tu, J., Dinh, A., Dinh, T.-N., 2002. The boiling crisis phenomenon: part I: nucleation and nucleate boiling heat transfer. Exp. Therm. Fluid. Sci. 26 (6-7), 775–792.
Tirelli, I., Ianiro, A., Discetti, S., 2023. An end-to-end KNN-based PTV approach for high-resolution measurements and uncertainty quantification. Exp. Therm. Fluid. Sci. 140, 110756.
Tolfts, O., Deplus, G., Machicoane, N., 2023. Statistics and dynamics of a liquid jet under fragmentation by a gas jet. Phys. Rev. Fluids. 8 (4), 044304.
Tolfts, O., Rack, A., Machicoane, N., 2024. Morphology and dynamics of the liquid jet in high-speed gas-assisted atomization retrieved through synchrotron-based high-speed X-ray imaging. Int. J. Multiphase Flow 181, 105004.
Tompkins, C., Prasser, H.-M., Corradini, M., 2018. Wire-mesh sensors: A review of methods and uncertainty in multiphase flows relative to other measurement techniques. Nucl. Eng. Des. 337, 205–220.
Topfer, F., Oberhammer, J., 2015. Millimeter-wave tissue diagnosis: the most promising fields for medical applications. IEEE Microw. Mag. 16 (4), 97–113.
Toral, H., 1981. A study of the hot-wire anemometer for measuring void fraction in two phase flow. J. Phys. e 14 (7), 822.
Torczynski, J., OHern, T., Shollenberger, K., Ceccio, S., Tassin, A., 1995. Finite Element Method Electrical Impedance Tomography for Phase Distribution Determination in Multiphase Flows: Validation Calculations and Experiments. Sandia National Lab (SNL-NM, Albuquerque, NM. Report No. SAND-95-1684C; CONF-960766-1.
Toschi, F., Bodenschatz, E., 2009. Lagrangian properties of particles in turbulence. Annu Rev. Fluid. Mech. 41, 375–404.
Toukan, A., Alexander, V., AlBazzaz, H., Al-Dahhan, M.H., 2017. Identification of flow regime in a cocurrent gas – liquid upflow moving packed bed reactor using gamma ray densitometry. Chem. Eng. Sci. 168, 380–390.
Toye, D., Marchot, P., Crine, M., L'Homme, G., 1996. Modelling of multiphase flow in packed beds by computer-assisted X-ray tomography. Measurem. Sci. Technol. 7 (3), 436–443.
Travis, K.N., Smith, S.E., Vignal, L., Djeridi, H., Bourgoin, M., Cal, R.B., Obligado, M., 2022. Characterization of coupling between inertial particles and turbulent wakes from porous disk generators. J. Fluid. Mech. 933, A42.
Tropea, C., Yarin, A.L., Foss, J.F., 2007. Springer Handbook of Experimental Fluid Mechanics. Springer.
Tryggvason, G., Scardovelli, R., Zaleski, S., 2011. Direct Numerical Simulations of Gas–Liquid Multiphase Flows. Cambridge University Press.
Ulucakli, M.E., Merte Jr., H., 1990. Nucleate boiling with high gravity and large subcooling. J. Heat. Transfer. 112 (2), 451–457.
Varga, C.M., Lasheras, J.C., Hopfinger, E.J., 2003. Initial breakup of a small-diameter liquid jet by a high-speed gas stream. J. Fluid. Mech. 497, 405–434.
Vejražka, J., Večeř, M., Orvalho, S., Sechet, P., Ruzicka, M.C., Cartellier, A., 2010. Measurement accuracy of a mono-fiber optical probe in a bubbly flow. Int. J. Multiphase Flow 36 (7), 533–548.
Vennemann, B., Rösgen, T., 2020. A dynamic masking technique for particle image velocimetry using convolutional autoencoders. Exp. Fluids. 61, 1–11.
Vericella, J.J., Baker, S.E., Stolaroff, J.K., Duoss, E.B., Hardin IV, J.O., Lewicki, J., Glogowski, E., Floyd, W.C., Valdez, C.A., Smith, W.L., 2015. Encapsulated liquid sorbents for carbon dioxide capture. Nat. Commun. 6 (1), 6124.
Vlasenko, A., Steele, E.C., Nimmo-Smith, W.A.M., 2015. A physics-enabled flow restoration algorithm for sparse PIV and PTV measurements. Measurem. Sci. Technol. 26 (6), 065301.
Vu, L., Machicoane, N., Li, D., Morgan, T.B., Heindel, T.J., Aliseda, A., Desjardins, O., 2023. A computational study of a two-fluid atomizing coaxial jet: validation against experimental back-lit imaging and radiography and the influence of gas velocity and contact line model. Int. J. Multiphase Flow 167, 104520.
Wang, G., Munoz-Ferreras, J.-M., Gu, C., Li, C., Gomez-Garcia, R., 2014. Application of linear-frequency-modulated continuous-wave (LFMCW) radars for tracking of vital signs. IEEE Trans. Microw. Theory Tech. 62 (6), 1387–1399.
Wang, H., Liu, Y., Wang, S., 2022a. Dense velocity reconstruction from particle image velocimetry/particle tracking velocimetry using a physics-informed neural network. Phys. Fluids 34 (1), 017116.
Wang, Z., He, F., Zhang, H., Hao, P., Zhang, X., Li, X., 2022b. Characterization of the in-focus droplets in shadowgraphy systems via deep learning-based image processing method. Phys. Fluids 34 (11), 113316.
Wu, Z., 2015. Developing a microwave tomographic system for multiphase flow imaging: advances and challenges. Trans. Institut. Measurem. Control 37 (6), 760–768.
Yamada, M., Saito, T., 2012. A newly developed photoelectric optical fiber probe for simultaneous measurements of a CO_2 bubble chord length, velocity, and void fraction and the local CO_2 concentration in the surrounding liquid. Flow Measurem. Instrument. 27, 8–19.
Yan, M., Ma, B., Tian, B., Hu, G., Wu, R., Wang, S., 2021. Design, simulation and reconstruction for a fast speed two-phase flow CT with ^{241}Am gamma ray sources. Ann. Nucl. Energy 151, 107970.
Yao, J., Takei, M., 2017. Application of process tomography to multiphase flow measurement in industrial and biomedical fields: A review. IEEE Sens. J. 17 (24), 8196–8205.
Yorkey, T.J., Webster, J.G., Tompkins, W.J., 1987. Comparing reconstruction algorithms for electrical impedance tomography. IEEE Trans. Biomed. Eng. (11), 843–852.
Young, C.J., Duke-Walker, V.O., McFarland, J.A., 2025. Droplet breakup and evaporation in liquid-fueled detonations. Exp. Therm. Fluid. Sci. 160, 111324.
Yuan, F., Yang, C., Zhong, P., 2015. Cell membrane deformation and bioeffects produced by tandem bubble-induced jetting flow. Proc. Natl. Acad. Sci. 112 (51), E7039–E7047.
Zenit, R., Koch, D.L., Sangani, A.S., 2001. Measurements of the average properties of a suspension of bubbles rising in a vertical channel. J. Fluid. Mech. 429, 307–342.
Zhang, D., Huang, H., Zhou, W., Feng, M., Zhang, D., Gao, L., 2024. Reconstruction of particle distribution for tomographic particle image velocimetry based on unsupervised learning method. Particuology 93, 349–363.
Zhang, L., Sun, M., Wang, T., Yang, L., Zhang, X., Zhao, J., Song, Y., 2022. An in-situ MRI method for quantifying temperature changes during crystal hydrate growths in porous medium. J. Therm. Sci. 31 (5), 1542–1550.
Zhang, W., Wang, Y., Lee, S.J., 2008. Simultaneous PIV and PTV measurements of wind and sand particle velocities. Exp. Fluids. 45 (2), 241–256.
Zhao, D., Guo, L., Lin, C., Zhang, X., 2005. An experimental study on local interfacial area concentration using a double-sensor probe. Int. J. Heat. Mass Transf. 48 (10), 1926–1935.
Zhao, F., Zhou, Z., Hung, D., Li, X., Xu, M., 2024. Flow field reconstruction from spray imaging: A hybrid physics-based and machine learning approach based on two-phase fluorescence particle image velocimetry measurements. Phys. Fluids 36 (4), 043316.
Zhao, L., Rezkallah, K., 1993. Gas-liquid flow patterns at microgravity conditions. Int. J. Multiph. Flow 19 (5), 751–763.
Zhu, L.-T., Chen, X.-Z., Ouyang, B., Yan, W.-C., Lei, H., Chen, Z., Luo, Z.-H., 2022. Review of machine learning for hydrodynamics, transport, and reactions in multiphase flows and reactors. Ind. Eng. Chem. Res. 61 (28), 9901–9949.